Systematic identification of cancer cell vulnerabilities to natural killer cell-mediated immune surveillance

Matthew F. Pech, Linda E. Fong, Jacqueline E. Villalta, Leanne J.G. Chan, Samir Kharbanda, Jonathon J. O'Brien, Fiona E. McAllister, Ari J. Firestone, Calvin H. Jan, Jeff Settleman[#]

Calico Life Sciences LLC, 1170 Veterans Boulevard, South San Francisco, CA, United States

[#]correspondence: jsettleman@gmail.com

Abstract

Only a subset of cancer patients respond to T-cell checkpoint inhibitors, highlighting the need for alternative immunotherapeutics. We performed CRISPR-Cas9 screens in a leukemia cell line to identify perturbations that enhance natural killer effector functions. Our screens defined critical components of the tumor-immune synapse and highlighted the importance of cancer cell interferon-γ signaling in modulating NK activity. Surprisingly, disrupting the ubiquitin ligase substrate adaptor DCAF15 strongly sensitized cancer cells to NK-mediated clearance. DCAF15 disruption induced an inflamed state in leukemic cells, including increased expression of lymphocyte costimulatory molecules. Proteomic and biochemical analysis revealed that cohesin complex members were endogenous client substrates of DCAF15. Genetic disruption of DCAF15 was phenocopied by treatment with indisulam, an anticancer drug that functions through DCAF15 engagement. In AML patients, reduced DCAF15 expression was associated with improved survival. These findings suggest that DCAF15 inhibition may have useful immunomodulatory properties in the treatment of myeloid neoplasms.

Introduction

Major advances in tumor control have recently been achieved by targeting immune inhibitory signaling pathways. Treatment with "checkpoint inhibitors," antibodies targeting PD1, PD-L1, or CTLA4, lead to durable responses across a wide range of indications, but only in a subset of patients. Treatment response is positively correlated with tumor mutational burden and infiltration of CD8+ effector T cells, which recognize tumor cells via peptides bound to major histocompatibility complex class I (MHC-I) molecules, suggesting that checkpoint inhibitors work best at clearing highly immunogenic cancers with repressed T cell responses [1-3]. Substantial efforts are being made to extend the benefits of immunotherapy to additional patients, including combining checkpoint inhibitors with other therapies, drugging additional lymphocyte-suppressive pathways, and boosting the activity of other arms of the immune system [4].

Resistance to therapy has long been a major problem in cancer treatment. Drugs targeting tumor growth pathways can profoundly reduce tumor burden, but resistance invariably arises, driven by the substantial genetic and phenotypic heterogeneity present within human tumors [5]. Recent clinical and experimental data have similarly highlighted the ability of cancer cells to escape checkpoint inhibitor-induced immune control. B2M and JAK1/2 mutations have been identified in melanoma patients with acquired resistance to checkpoint inhibitors [6,7]. These mutations impair recognition of the tumor by the adaptive immune system, either by directly disrupting antigen presentation or by rendering the cells insensitive to IFNγ, an important inducer of MHC-I expression. Functional genetic screens using T cell-cancer cell cocultures have highlighted similar mechanisms of resistance *in vitro* [8-11]. Even treatment-naïve tumors can be highly immuno-edited, presenting with IFNγ pathway mutations, reduced MHC-I expression and loss of the peptide sequences that can serve as antigens [12-15]. Together, these findings highlight a critical need for therapies that can either increase MHC expression or work in a MHC-independent fashion.

Anti-tumor immunity is not solely mediated by the adaptive immune compartment. Innate immune cells, most notably natural killer (NK) cells, can have both direct tumoricidal activity and also help to fully elaborate long-lasting anti-tumor responses [16-19]. NK cells are cytotoxic lymphocytes capable of mounting rapid responses to damaged, infected, or stressed cells, including cancer cells.

58 T and NK cells share effector functions, releasing cytokines and exocytosing lytic granules upon
59 activation to kill target cells. However, NK activation status is controlled by the integrated signals
60 from germline-encoded NK-activating and -inhibiting receptors (aNKRs/iNKRs). Generally,
61 iNKR ligands are expressed by normal and healthy cells, whereas aNKR ligands are upregulated
62 after DNA damage or viral insult [19,20]. MHC-I molecules provide a potent inhibitory signal sensed
63 by NK cells, enabling the innate immune system to respond productively to MHC-deficient cells.
64 As a result, there is considerable interest in amplifying NK responses to cancers, as well as
65 developing NK-based cell therapies [18-20].
66
67 Here, we performed genetic screens in an MHC-deficient leukemic cell line to systematically
68 identify modulators of NK-mediated anti-cancer immunity. These screens, unexpectedly, revealed
69 the potential therapeutic utility of targeting the CRL4 substrate adaptor DCAF15 in myeloid
70 malignancies. Disruption of DCAF15 strongly sensitized cancer cells to NK-mediated killing,
71 resulting from increased cancer cell expression of lymphocyte costimulatory molecules. Proteomic
72 experiments revealed that DCAF15 interacted with and promoted the ubiqitination of the cohesin
73 complex members. Treatment with indisulam, an anticancer drug that modulates DCAF15
74 function, reduced interaction with cohesin members and mimicked DCAF15 loss-of-function
75 immunophenotypes.
76
77 **Results**
78
79 **A genome-scale CRISPR screen identifies modulators of NK effector functions**
80
81 We performed genome-scale CRISPR screens in K562 cells to identify perturbations that modulate
82 NK-92-mediated killing (Figure 1A). K562 human chronic myelogenous leukemia cells are a NK-
83 sensitive cancer cell line that weakly expresses MHC-I. For screening purposes, a clonal isolate of
84 K562 cells expressing high levels of spCas9 was generated and validated (Figure 1- figure
85 supplement 1A-C). NK-92 cells are a human lymphoma-derived cell line phenotypically similar
86 to activated NK cells.[21] These cells exhibit interleukin-2 (IL-2)-dependent growth, express a large
87 number of aNKRs and few iNKRs [22], and display potent cytolytic activity against K562 cells.
88

89 In pilot experiments, labeled K562 cells were co-cultured with NK-92 cells to determine an
90 effector-to-target (E:T) ratio that applied sufficient selective pressure for screening (Figure 1-
91 figure supplement 1D-F). IL-2 was removed during the co-culture to promote the eventual death
92 of NK-92 cells, allowing the collection of genomic DNA preparations undiluted by effector cell
93 DNA. A multi-day timeframe between the NK-92 challenge and screen readout was used to
94 capture tumor cell fitness changes related both to the direct cytolytic activities of NK cells as well
95 as the longer-term effects from NK-released cytokines.
96
97 For the co-culture screen, cas9-expressing K562 cells were infected with a genome-scale single
98 guide RNA (sgRNA) library targeting all unique coding genes and miRNAs, as well as one
99 thousand non-targeting controls (Table S2). Seven days post-infection, cells were either grown
100 normally or challenged with NK-92 cells at a 1:1 or 2.5:1 E:T ratio, reducing K562 cell counts 19-
101 fold or 43-fold, respectively, by the end of the screen (Figure 1B). Deep sequencing was used to
102 compare changes in sgRNA abundance between the challenged and unchallenged state after 8 days
103 of co-culture, and genes were ranked using the MAGeCK software [23]. (Figure 1C, Table S2) There
104 was good agreement between the results from screens performed at the different E:T ratios (Figure
105 1- figure supplement 2).
106
107 The screen revealed two broad classes of "hits"— sgRNAs targeting components of the tumor-
108 immune synapse or components of the IFNγ signaling pathway (Figure 1C-D). Disruption of
109 ICAM1 was the top-ranked NK-92 evasion mechanism, scoring many orders of magnitude
110 stronger than any other gene—an observation consistent with the critical role of ICAM1-LFA1
111 interactions in establishing initial target-lymphocyte adhesion and polarizing cytotoxic granules
112 towards the synapse [16]. Single guide RNAs targeting multiple other tumor-immune synapse
113 components were also enriched after NK-92 challenge, including NCR3LG1 (#26-ranked gene by
114 MaGeCK score), the activating ligand for NKP30 on NK cells [24]; CD58 (#37), an adhesion
115 molecule that binds CD2 [25,26] ; and CD84 (#80), a SLAM-related receptor that binds homotypically
116 to promote activation and cytokine secretion in lymphocytes [27-29]. Other than NECTIN2, sgRNAs
117 targeting NK-inhibitory surface proteins did not score prominently as NK-sensitization
118 mechanisms, consistent with the weak MHC-I expression on K562 cells and the limited repertoire
119 of NK inhibitory receptors expressed on NK-92 cells [22]. NECTIN2 transmits both stimulatory or

120 inhibitory signals to NK cells, depending on whether it is bound to DNAM1 (CD226) or TIGIT,
121 respectively [30,31].
122
123 After ICAM1, the top 10 highest scoring NK-92 evasion mechanisms were dominated by sgRNAs
124 targeting the proximal components of the IFNγ signaling pathway, including STAT1, JAK1,
125 IFNGR2, JAK2 and INFGR1 (Figure 1D). Consistent with the importance of cancer cell IFNγ
126 signaling, sgRNAs targeting negative regulators of the interferon response were strongly depleted
127 after NK-92 challenge. Disruption of the protein tyrosine phosphatases PTPN2 and PTPN1 were
128 the #2 and #5 ranked NK-92 -sensitizing mechanisms, respectively. Presumably, these proteins
129 suppress IFNγ-induced immunomodulation by dephosphorylating STAT and JAK proteins, as has
130 been reported in CRISPR screens using T-cell coculture systems or syngeneic tumor models [9,10].
131 Taken together, these findings indicate that our *in vitro* functional genomics screens effectively
132 revealed known components of physiologically-relevant immune synapse and cytokine pathways.
133
134 **Prospective identification of novel genes affecting sensitization to NK cells**
135
136 Mechanisms of NK-92 sensitization identified in the screen were diverse, revealing many strongly-
137 scoring genes not previously linked to either interferon signaling or NK cell biology (Figure 1).
138 Most surprisingly, the top-ranked mechanism for promoting NK-92 mediated clearance was
139 disruption of DCAF15, an uncharacterized substrate adaptor for CRL4 ubiquitin E3 ligases.
140 DCAF15 is a member of the large family of DDB1 and Cul4-associated factors (DCAFs) [32]. CRL4
141 complexes enable cells to mark proteins for proteosomal degradation, helping regulate intracellular
142 protein homeostasis. As substrate adaptors for CRL4, DCAF proteins provide specificity to the
143 complex, determining which client proteins are ubiquitinated [33]. As with most substrate adaptors,
144 the normal client repertoire of DCAF15 is undefined, and relatively little is known about the
145 biological function of DCAF15.
146
147 We also noted that disruption of two cohesin-related genes, STAG2 and HDAC8, scored as NK-
148 92 sensitization factors (ranked #26 and #19, respectively). Cohesin is a ring-shaped complex
149 involved in chromatin replication, organization and repair, with STAG2 acting as a core complex
150 member and HDAC8 controlling chromatin accessibility [34]. Cohesin dysregulation has cell

151 context-specific consequences, including DNA damage and aneuploidy; in leukemic cells, cohesin
152 mutations are thought to enforce stem cell programs by altering chromatin organization [35].
153
154 **A phenotypic screen based on MHC-I upregulation to identify modulators of the**
155 **IFNγ response**
156
157 The prominent role for IFNγ signaling in the immune response to cancer cells, both clinically and
158 in our screens, prompted us to define more specifically which NK-92-sensitizing genes are
159 involved in modulating the IFNγ response. MHC-I levels are highly upregulated in K562 cells
160 after IFNγ exposure, increasing 5.9+/-0.98 fold after 24hrs of exposure to IFNγ. This induction
161 was dependent on STAT1 and was nearly doubled by disrupting PTPN2 (Figure 2A-B and Figure
162 2- figure supplement 1). We therefore used IFNγ-induced cell surface MHC-I expression as a
163 proxy for the strength of the interferon response. K562 cells transduced with a genome-scale
164 CRISPR library were treated with IFNγ for 24hrs and MHC-I expression was measured by flow
165 cytometry. The brightest 20% and dimmest 20% of cells were sorted, and deep sequencing was
166 used to compare sgRNA abundance between the populations (Figure 2C, Table S3).
167
168 As expected, cells with impaired MHC-I upregulation were highly enriched for sgRNAs targeting
169 the IFNγ-JAK-STAT pathway (IFNGR1/2, JAK1/2, STAT1, IRF1/2), as well as the antigen
170 processing/presentation machinery (B2M, TAP1/2, TAPBP, PDIA3, HLA-C/B) (Figure 2D).
171 Conversely, disruption of PTPN2 or STAG2 induced an exuberant MHC-I response. Surprisingly,
172 sgRNAs targeting epigenetic factors were highly enriched within the brightest MHC-I expressing
173 cells—most prominently, members of the BCOR complex PCGF1 and KDM2B, members of the
174 PRC2 complex EZH2 and SUZ12, as well as factors affecting histone methylation/acetylation
175 status.
176
177 Rank-rank comparisons between the NK and MHC screens were informative in prospectively
178 defining a core group of IFNγ response genes in K562 cells (Figure 2E). Comparing sgRNAs
179 enriched after NK-92 challenge with those causing impaired MHC-I upregulation clearly
180 delineated the known proximal components of the IFNγ signaling pathway (IFNGR1/2, JAK1/2,

181 STAT1), and highlighted several poorly characterized genes such as GSE1, SPPL3 and NR2F2
182 (Figure 2E).
183
184 Surprisingly, comparing sgRNAs depleted after NK-92 challenge with those causing an
185 exaggerated MHC-I response highlighted the CRL4 substrate adaptor DCAF15 most prominently,
186 alongside the cohesin members STAG2 and HDAC8 (Figure 2E). As expected, negative feedback
187 regulators of the IFNγ pathway (PTPN1 and PTPN2) were also recovered by this analysis. We
188 focused additional studies on understanding the function of DCAF15, given its prominence in both
189 the NK sensitization (#1 ranked hit at 2.5 E:T ratio; #12 ranked hit at 1:1 E:T ratio) and MHC
190 upregulation (#13 ranked hit) screens.
191
192 **Disruption of DCAF15 enhances NK effector functions**
193
194 To evaluate hits from the CRISPR screens, we generated individual gene knockout (KO) cell lines
195 by lentiviral sgRNA expression, producing polyclonal cell lines with high levels of gene disruption
196 (Figure 2- figure supplement 1 and Figure 3-figure supplement 1). Fluorescently-labeled control
197 or test KO target cell lines were subjected to competitive co-culture assays in the presence of either
198 NK-92 or primary NK effector cells, with changes in the relative ratios of target cell types
199 measured over time by flow cytometry (Figure 3A).
200
201 As expected, disrupting ICAM1 in K562 cells conferred very high levels of protection against NK-
202 92 cells (Figure 3B-C; 19.7-fold enrichment). Disabling signaling downstream of IFNγ by
203 disrupting STAT1 provided an intermediate level of resistance (2.45-fold enrichment). K562s are
204 very sensitive to NK-mediated killing, providing a large dynamic range for detection of resistance-
205 promoting factors, while limiting the ability of the assay to detect similarly large increases in
206 sensitization. Nevertheless, multiple independent sgRNAs targeting DCAF15 promoted
207 sensitization to NK-92 cells (1.6-fold depletion), with a similar degree of preferential killing
208 observed for NECTIN2 or PTPN2 KO cells (NECTIN2: 1.95-fold depletion; PTPN2: 1.4-fold
209 depletion).
210

211 We repeated NK-92 competitive co-culture experiments after disruption of DCAF15, PTPN2,
212 STAT1 and ICAM1 in Daudi cells, a B2M-deficient B-cell lymphoma line (Figure 3D, Figure 3-
213 figure supplement 1D-F). ICAM1 KO Daudi cells were highly protected against NK-92 cell
214 killing, whereas disruption of DCAF15 or PTPN2 led to enhanced killing. In contrast to K562
215 cells, STAT1 disruption in Daudi cells promoted their preferential killing.
216
217 To extend these observations to primary NK cells, human peripheral NK cells were isolated from
218 PBMCs of 6 healthy donors, activated and challenged in competitive co-cultures with various
219 K562 KO cell genotypes (Figure 3E and Figure 3- figure supplement 2). Disruption of DCAF15
220 or PTPN2 promoted sensitization to primary NK cells, albeit with reduced magnitudes of effect
221 compared to NK-92 cells (PTPN2: 1.3-fold depletion; DCAF15: 1.15-fold depletion). In 3 out of
222 6 donors, NK cells showed increased degranulation, as measured by cell surface CD107a
223 expression, when challenged with DCAF15 KO cells (Figure 3F). ICAM1 disruption promoted
224 resistance to NK cell attack, but only conferred partial protection (2.3-fold enrichment). The effect
225 of STAT1 disruption was extremely variable, with STAT1 KO K562 cells strongly preferentially
226 killed by primary NK cells from a subset of donors. These findings implicate DCAF15 and PTPN2
227 as novel modulators of NK-mediated cancer cell immunity.
228
229 **Loss of the cullin-RING E3 ligase substrate adaptor DCAF15 leads to an inflamed state**
230 **distinct from dysregulated IFNγ signaling**
231
232 DCAF15 was a strong hit in both the NK sensitization and MHC upregulation screens, suggesting
233 that DCAF15 disruption sensitizes K562 cells to NK-mediated killing by dysregulating the IFNγ
234 response. Consistent with the screening results, polyclonal K562 cells expressing DCAF15
235 sgRNAs ("DCAF15 KO cells") displayed 2.45-fold higher levels of MHC-I than control knockout
236 cells after 24hrs of IFNγ exposure, an effect comparable in magnitude to PTPN2 disruption (Figure
237 4A). We then tested whether DCAF15 KO cells exhibited hallmarks of dysregulated JAK-STAT
238 signaling, using PTPN2 KO cells as a positive control. We were unable to see any difference in
239 induction of STAT1 phosphorylation after IFNγ exposure in DCAF15 KO cells, or differences in
240 steady state levels of STAT1/2, JAK1/2 or IFNGR1 (Figure 4B and data not shown). DCAF15 KO
241 cells appeared healthy and proliferated at a normal rate (Figure 4 – figure supplement S1A). As in

242 wild-type K562 cells, long-term IFNγ exposure was neither cytotoxic nor cytostatic to DCAF15
243 KO cells (Figure 4c and [36]). In contrast, PTPN2 KO cells showed higher levels of STAT1^{PY701}
244 induction after IFNγ exposure, and their proliferative rate was temporarily reduced after transient
245 exposure to IFNγ, or more substantially slowed down by continuous treatment with the cytokine
246 (Figure 4B-C).
247
248 We explored the transcriptional and immunophenotypic response of cells to IFNγ treatment. RNA-
249 seq and flow cytometry was performed on control, DCAF15 KO or PTPN2 KO K562 cells basally
250 and after 24hrs of IFNγ exposure. Wild-type cells dramatically upregulated transcription of anti-
251 viral genes and components of the antigen processing and presentation pathway after IFNγ
252 treatment (Figure 4 – figure supplement 1B and Table S4). On the cell surface, K562 cells
253 exhibited STAT1-dependent upregulation of ICAM1 expression after IFNγ treatment, with a
254 variety of other important NK ligands unaffected by cytokine treatment (Figure 4- figure
255 supplement 1C).
256
257 Clustering analysis clearly showed that PTPN2 KO cells were transcriptionally distinct from
258 control or DCAF15 KO cells both before and after cytokine exposure (Figure 4D). In the basal
259 state, PTPN2 KO cells were enriched for inflammation and interferon-associated Gene Ontology
260 (GO) terms (Figure 4 – figure supplement 1D). After cytokine exposure, gene set enrichment
261 analysis revealed that PTPN2 KO cells had exaggerated transcriptional responses to interferon and
262 were also enriched for apoptotic GO gene categories (Figure 4 – figure supplement 1E). PTPN2
263 KO cells also showed greater IFNγ-induced MHC-I and ICAM1 cell surface expression (Figure
264 2A and Figure 4 – figure supplement 1C). These results suggest that loss of appropriate IFNγ
265 negative feedback may both promote cell death and modulate NK cell interactions.
266
267 In contrast, DCAF15 KO cells did not show substantial differences in their transcriptional response
268 to IFNγ (Figure 4D). However, DCAF15 KO cells were enriched for GO terms associated with
269 NK-mediated cytotoxicity, antigen presentation and cell adhesion, consistent with our phenotypic
270 characterization of these cells (Figure 4E). Together, these findings indicate that while DCAF15

271 KO K562 cells exhibit a relatively normal response to IFNγ stimulation, they are nonetheless in
272 an inflamed state primed to interact with cytotoxic lymphocytes.
273
274 **DCAF15 knockout cells enhance NK-92 triggering via CD80 expression**
275
276 Intriguingly, differential expression analysis showed that one of the most significantly upregulated
277 genes in DCAF15 KO K562 cells was CD80 (Figure 4F; Q value 3.7e-23, Beta value 0.98). CD80
278 is an important co-stimulatory molecule for lymphocytes, regulating T cell activation and tolerance
279 by ligation to CD28, CTLA4 or PDL1 [37]. During antigen-presenting cell (APC) activation, the
280 upregulation of MHC molecules and CD80 provide critical antigenic and costimulatory signals to
281 T cells [38]. K562 cells are an undifferentiated and multipotential CML cell line, well-studied for
282 their ability to differentiate towards many different lineages, including APC-like states [39]. We
283 hypothesized that upregulation of MHC-I and CD80 in DCAF15 KO cells may reflect a broader
284 acquisition of APC-like properties. Indeed, immunophenotyping of unstimulated DCAF15 KO
285 cells revealed higher levels of the APC markers CD80, CD40 as well as class I and II MHC
286 molecules (Figure 5A; 2.23-fold CD80 increase; 2.01-fold CD40 increase; 1.44-fold MHC-I
287 increase; 1.22-fold MHC-II increase). DCAF15 KO cells did not display higher levels of the APC
288 maturation marker CD83 (Figure 5A). Expression levels of B7H6, ICAM1, ULBP2/5/6, IFNGR1,
289 CD58 and NECTIN2 were either unaltered in DCAF15 KO cells or modestly changed in a fashion
290 not expected to increase sensitivity to NK cells (Figure 5 – figure supplement 1A). Importantly,
291 the changes to the DCAF15 KO cell immunophenotype could be rescued by constitutive
292 expression of a sgRNA-resistant DCAF15 open-reading frame (Figure 5 – figure supplement 1B-
293 D).
294
295 Transducing tumors with the B7 ligands CD80 or CD86 can enhance anti-tumor immunity by
296 enabling the tumor cells to directly deliver antigenic and costimulatory signals to T and NK cells
297 [40-43]. While best understood in the context of T cell biology, B7 ligands have been shown to
298 promote NK activation, via CD28-dependent and -independent pathways [42-46]. We confirmed that
299 NK-92 cells are CD28-positive, whereas we could not detect CD28 on peripheral CD3- CD56+
300 NK cells (Figure 5 – figure supplement 1E-F). K562 cells stably over-expressing wild-type CD80
301 were generated (Figure 5B; 49-fold higher CD80 levels than endogenous). Over-expression was

302 sufficient to increase K562 sensitivity to NK-92 mediated killing (Figure 5C), whereas
303 overexpression of a mutant form of CD80 carrying point mutations that abrogate CD28 binding [47]
304 ($CD80^{Q65A,M72A}$) had no effect.
305
306 We next determined whether the increased CD80 expression in DCAF15 KO cells was important
307 for their altered NK-92 sensitivity. Changes in NK-92 degranulation were measured after
308 incubation with K562 cells pretreated with either control or CD80 blocking antibodies (Figure
309 5D). As expected, ICAM1 KO cells triggered less NK-92 degranulation than control cells (by
310 52±12%) and were not significantly affected by CD80 antagonism (Figure 5E). DCAF15 KO cells
311 showed a 17±8% increased ability to trigger NK-92 cells and were approximately twice as
312 sensitive to CD80 antagonism compared to control cells (Figure 5E-F). Following CD80
313 antagonism, degranulation triggered by DCAF15 KO was not significantly different from
314 untreated control cells. Taken together, these results indicate that DCAF15 disruption in K562
315 cells induces an APC-like immunophenotype conducive to promoting lymphocyte responses, with
316 higher CD80 expression especially important for increased NK-92 cell triggering.
317
318 **The anti-leukemia drug indisulam inhibits DCAF15 function**
319
320 Aryl sulfonamide drugs have demonstrated promising anti-cancer properties in hematological
321 malignancies [48]. Recently, it was discovered that these agents work by binding DCAF15 and
322 redirecting the ubiquitination activity of the CRL4-DCAF15 E3 ligase towards the essential
323 splicing factor RBM39 [49,50]. This mechanism of action is conceptually similar to that of the "IMiD"
324 thalidomide analogs, which promote the degradation of various lymphocyte transcription factors
325 by engaging the CRL4-cereblon E3 ubiquitin ligase [51-53]. Presumably, sulfonamides and IMiDs
326 also impair the degradation of the normal client proteins when they induce neomorphic activity of
327 the substrate adaptor. This has not been proven, however, as it is difficult to systematically
328 determine the normal substrate repertoire of adaptor proteins.
329
330 We hypothesized that treating cells with low concentrations of the aryl sulfonamide indisulam
331 would phenocopy DCAF15 depletion (Figure 6A). Three-day dose-response experiments revealed
332 that K562 cells were sensitive to indisulam, and that DCAF15 disruption reduced this sensitivity,

333 consistent with previous reports[50] (Figure 6B). Dose-response experiments across a panel of 16
334 hematological cancer cell lines confirmed the reported positive relationship between DCAF15
335 mRNA expression levels and indisulam sensitivity [49] (Figure 6 – figure supplement 1A; R^2=0.33,
336 P=0.02).
337
338 We empirically determined that 100nM indisulam treatment moderately lowered RBM39 levels
339 while minimally affecting cell viability and proliferation over a four-day period (Figure 6C-D and
340 [50]). Remarkably, this treatment regime was able to recapitulate the increased CD80 expression
341 seen in K562 DCAF15 KO cells (Figure 6E; 2.14-fold increase), and more modestly, the effects
342 on MHC-I and CD40 expression (1.36-fold and 1.27-fold increase, respectively). CD80
343 upregulation was first detected 24hrs after treatment initiation and plateaued after 48hrs (Figure 6
344 – figure supplement 1B). Importantly, indisulam treatment did not further upregulate CD80 in
345 K562 DCAF15 KO cells, suggesting that the pharmaco-modulation of CD80 levels was entirely
346 mediated through DCAF15 (Figure 6F).
347
348 To extend these observations to other cell lines, a panel of hematological cancer cell lines was
349 screened to identify those with detectable CD80 expression (Figure 6 – figure supplement 1C).
350 The CML cell line KU812 expressed similar levels of CD80 as K562, whereas the Daudi
351 lymphoma cell line expressed significantly higher basal CD80 levels. These cells lines were
352 subjected to similar 4-day low-dose regimes of indisulam, which only modestly affected the
353 growth and viability of the cells (Figure 6 – figure supplement 1D). Both Daudi and KU812 cells
354 up-regulated CD80 levels after indisulam treatment (Figure 6G; 2.45-fold for Daudi, 1.71-fold for
355 KU812). Indisulam was not able to induce *de novo* CD80 expression in CD80-negative cell lines
356 (Figure 6 – figure supplement 1E). Thus, in certain cellular contexts, aryl sulfonamides are
357 immuno-modulatory agents that alter co-stimulatory protein levels by disrupting the normal
358 functions of DCAF15.
359
360 **Reduced DCAF15 expression is associated with improved survival in AML patients**
361
362 Given the *in vitro* findings, we hypothesized that lower DCAF15 expression in myeloid
363 malignancies could be associated with better clinical outcomes. We tested this hypothesis using

364 publicly available acute myeloid leukemia (AML) datasets [54,55]. In both adult and pediatric AML,
365 lower expression of DCAF15 mRNA was associated with increased median overall survival time
366 (Figure 6H-I). The improved survival of DCAF15-low patients was not driven by a correlation
367 between DCAF15 expression and more aggressive AML subtypes (Figure 6 – figure supplement
368 1F-G). Taken together, these findings indicate that lower DCAF15 function, achieved
369 pharmacologically or by genetic means, is associated with favorable immunophenotypes *in vitro*
370 and improved outcomes in AML patients.
371
372 **Cohesin complex members are CRL4-DCAF15 E3 ligase client proteins**
373
374 The normal substrate repertoire of DCAF15 is unknown. To systemically identify direct DCAF15
375 client proteins, we undertook proximity-based proteomic analysis of DCAF15 interaction partners
376 (Figure 7A). DCAF15 was fused to a promiscuous bacterial biotin ligase [56] ("DCAF15-BioID")
377 and stably expressed in K562 cells, enabling recovery of interaction partners by streptavidin pull-
378 down. We first confirmed that exogenous C-terminally tagged DCAF15 was able to rescue
379 DCAF15 KO phenotypes and associate with CRL4 complex members DDB1 and CUL4A (Figure
380 5 – figure supplement 1B-D and Figure 7 – figure supplement 1A). During stable DCAF15
381 overexpression, we observed that the basal concentration of biotin in the media (~3μM) was
382 sufficient to induce BioID activity in the absence of exogenous (50μM) biotin supplementation
383 (Figure 7B). However, proteasome inhibition by MG132 increased accumulation of DCAF15-
384 BioID and biotinylated species. As a control, results were compared to a GFP-BioID fusion,
385 expected to generically biotinylate proteins. GFP-BioID accumulated much more readily than
386 DCAF15-BioID, and its biotinylation activity was not affected by MG132 treatment.
387
388 After 24hrs of biotin and MG132 treatment, biotinylated protein species were recovered under
389 stringent denaturing conditions. Isobaric labeling and mass spectrometry were used to
390 quantitatively compare the DCAF15 interactome to the GFP interactome (Figure 7C and Table
391 S5). This approach clearly recovered DCAF15 and the core CRL4 complex, including DDA1,
392 DDB1 and CUL4A (DCAF15: 155.6-fold change, P=2.5e-152; DDA1: 24.5-fold change, P=6.5e-
393 139; DDB1: 4.86-fold change, P=8.1e-21; CUL4A: 3.8-fold change, P=8.5e-18).
394

395 Surprisingly, two of the most differentially biotinylated proteins were the cohesin complex
396 members SMC1A and SMC3 (SMC1: 2.39-fold change, P=0.00098; SMC3: 2.76-fold change,
397 P=5e-5). We confirmed the interaction between DCAF15-BioID and endogenous SMC1 and 3 by
398 streptavidin-pulldown followed by western blotting (Figure 7D). To determine whether this
399 association with cohesin was a generic feature of CRL4 complexes or specific to the CRL4 loaded
400 with DCAF15, we examined the interaction partners of a different substrate adaptor. DCAF16 is
401 a nuclear-localized CUL4 substrate adaptor, which, like DCAF15, interacts with DDB1 despite
402 lacking a canonical WD40 docking domain [32]. When stably expressed in K562 cells, DCAF16-
403 BioID fusions accumulated similarly to DCAF15-BioID, interacted with DDB1 but did not
404 biotinylate SMC proteins (Figure 7E). As low concentrations of indisulam phenocopy certain
405 aspects of DCAF15 depletion (Figure 6), we asked whether indisulam treatment would alter the
406 interaction of DCAF15 with cohesin. DCAF15-BioID cells were pre-treated with indisulam for
407 72hrs prior to biotin and MG132 addition. This treatment regime lead to substantial indisulam-
408 dependent biotinylation of RBM39 and reduced recovery of biotinylated SMC proteins (Figure
409 7E).
410
411 To test whether DCAF15 promoted SMC1 ubiquitination, we co-transfected 293T cells with his-
412 tagged ubiquitin, DCAF15 and SMC1A, and purified ubiquitinated species under denaturing
413 conditions by nickel affinity chromatography. Co-expression of DCAF15, but not GFP, led to the
414 recovery of poly-ubiquitinated SMC1A (Figure 7F). Treatment with indisulam reduced the amount
415 of ubiquitinated SMC1A recovered. These orthogonal proteomic and biochemical assays support
416 the notion that cohesin proteins are *bona fide* client ubiquitination substrates for DCAF15, with
417 these interactions impaired by DCAF15-engaging aryl sulfonamide drugs.
418
419 **Discussion**
420
421 Clinical and experimental data have revealed that disrupting optimal antigen presentation levels is
422 a common mechanism by which cancer cells escape recognition by the adaptive immune system.
423 We performed CRISPR-Cas9 screens using NK-92:K562 co-cultures to uncover perturbations that
424 enhance natural killer mediated anti-cancer immunity. We discovered and characterized how
425 disruption of DCAF15 or PTPN2 sensitizes a variety of cancer cell types to both NK-92 and

426 primary NK cells. In addition, the screens clearly identified known lymphocyte adhesion factors
427 and aNKR/iNKR ligands, such as ICAM1, NCR3LG1, CD58, CD84 and NECTIN2. Performing
428 additional genetic screens on diverse cancer cell lines and natural killer subtypes will enable a
429 more complete understanding of the relative importance of various aNKRs and iNKRs and should
430 identify novel immunotherapeutic targets.
431
432 There was a strong IFNγ signature within our NK-92:K562 screens. We determined that disruption
433 of PTPN2, a negative regulator of IFNγ signaling, consistently enhanced NK cell sensitivity.
434 Interestingly, preventing cancer cell IFNγ signaling had a much more variable effect than removing
435 negative feedback on the pathway, promoting resistance or sensitization to NK cells in target and
436 effector cell dependent manner. This variability likely reflects the complexity of cancer cell IFNγ
437 signaling, which can include MHC upregulation, growth suppression and immunomodulation.
438
439 In K562 cells, PTPN2 KO rendered IFNγ treatment growth suppressive, likely through the
440 induction of apoptosis, while also enhancing the immunomodulatory effects of the cytokine. The
441 immunophenotypic changes include enhanced MHC-I expression, which likely inhibits full
442 activation of NK cell cytotoxicity, especially in primary NK cells that express a broader KIR
443 repertoire than NK-92 cells [22]. PTPN2 disruption has previously been shown to enhance activated
444 T-cell mediated killing, as well as potentiate the effect of immunotherapy in syngeneic tumor
445 models [9,10,57]. These data suggest that targeting PTPN2 may be a generalizable strategy to sensitize
446 tumor cells to multiple arms of the immune system.
447
448 The importance of the cancer cell IFNγ response prompted us to systemically identify
449 perturbations that modulated IFNγ signaling, as read out by cytokine-induced MHC-I
450 upregulation. As expected, this screen clearly delineated the proximal components of the IFNγ-
451 JAK-STAT pathway, as well as the antigen processing/presentation machinery. Surprisingly,
452 disruption of DCAF15, a poorly characterized substrate adaptor for the CRL4 E3 ligase, was a top
453 scoring hit in both the MHC-I and NK screens. We therefore focused our efforts on understanding
454 the role of DCAF15 in this context. We determined that DCAF15 KO cells did not have a grossly
455 dysregulated response to IFNγ, but scored in the MHC-I screen due to higher unstimulated levels
456 of MHC-I. This change reflected a broader phenotypic switch in DCAF15 KO cells reminiscent

457 of APC activation, including the upregulation of a variety of co-stimulatory and antigen-presenting
458 molecules (Figure 7G). Higher CD80 levels in DCAF15 KO cells were especially important for
459 increasing NK-92 cell triggering. Cross-talk between APCs and NK cells is a well-established
460 phenomenon that mutually regulates both cell types [58]. These interactions, which often occur at
461 sites of inflammation or secondary lymphoid organs, can promote APC maturation or lysis in a
462 context-dependent fashion. Further work is needed to determine whether DCAF15 plays a role in
463 the activation of APCs and their interactions with NK cells.
464
465 Our data suggest that the surface factors upregulated by DCAF15 disruption are not direct client
466 proteins of the substrate receptor, but rather represent events secondary to altered turnover of the
467 normal DCAF15 client protein(s). We pioneered a novel approach to systemically purify substrates
468 of DCAF family members, as conventional biochemical methods are poorly suited to recover the
469 transient, low-affinity interactions between substrate adaptors and client proteins. The use of
470 DCAF-BioID fusion proteins and proteasome inhibition protects labile substrates from
471 degradation and robustly recovers biotinylated proteins under stringent, denaturing conditions. We
472 anticipate this will be a generalizable strategy for discovering client proteins for the whole family
473 of CUL4 CRL substrate receptors.
474
475 Proteomic analysis and subsequent validation experiments showed that DCAF15 loaded into
476 CLR4 complexes, interacted with cohesin complex members SMC1 and SMC3, and promoted
477 their ubiquitination. We were intrigued by these interactions given the similar CRISPR screening
478 scoring pattern of DCAF15 to the cohesin factors STAG2 and HDAC8 (Figure 2E); the shared
479 roles of cohesin and CRL4 E3 ligases in DNA metabolism, organization, replication and repair
480 [34,59,60]; and the ability of cohesin mutations to dysregulate hematopoietic differentiation in myeloid
481 malignancies [35]. Rather than globally controlling SMC protein levels, we speculate that CRL4-
482 DCAF15 complexes ubiquitinate cohesin at specific genomic sites to regulate chromatin topology
483 or repair (Figure 7G). In this model, disruption of either STAG2, HDAC8 or DCAF15 impair
484 cohesin function with overlapping phenotypic consequences. Further work is needed to elaborate
485 the control of cohesin function by DCAF15 and how this may promote APC-like differentiation.
486

487 Recently, it was discovered that aryl sulfonamide drugs including indisulam are capable of binding
488 to DCAF15 and altering CRL-DCAF15 substrate specificity towards the splicing factor RBM39
489 [49,50]. The cytotoxic effects of indisulam were driven by splicing defects resulting from RBM39
490 degradation. Our studies confirmed indisulam-induced RBM39 degradation and the indisulam-
491 dependent interaction between DCAF15 and RBM39. We also discovered indisulam-induced
492 phenotypes attributable to inhibition of DCAF15's normal functions. Concentrations of indisulam
493 with limited RBM39 degradation or cytotoxicity had immunomodulatory properties that
494 phenocopied genetic DCAF15 disruption. Biochemically, the recruitment of endogenous client
495 proteins to CRL4-DCAF15 and subsequent ubiquitination was impaired by indisulam treatment.
496 We also determined that AML patients with naturally occurring lower levels of DCAF15 had
497 improved overall survival. While these clinical data are preliminary in nature, they provide a
498 rationale for drugging DCAF15 in myeloid neoplasms, achieved through judicious dosing of
499 existing anti-cancer sulfonamides or the development of pure DCAF15 inhibitors.
500
501

502 **FIGURES**

503 **Figure 1. A genome-scale CRISPR screen identifies modulators of NK effector functions**

504 A) Overview of the genome-scale NK CRISPR screening system.

505 B) K562 population doublings (PDs) during the CRISPR screen, as measured by total number
506 of live cells. Note that early timepoints from the co-culture reflect the presence of both
507 K562 and NK-92 cells.

508 C) Analysis of the NK CRISPR screen results. Changes in sgRNA abundance were compared
509 between the 2.5:1 E:T co-culture condition and day 15 dropout cells using the MAGeCK
510 algorithm. The top 10 enriched or depleted genes are shown, as rank-ordered by MAGeCK
511 score; other manually selected genes are highlighted with their rank indicated. FDR, false
512 discovery rate.

513 D) Overview of high-scoring components of the tumor-immune synapse and IFNγ signaling
514 pathway recovered by the screen. sgRNAs against genes enriched after exposure to NK-92
515 cells are marked in red, while depleted sgRNAs are marked in blue.

516

517 **Figure 1 – figure supplement 1. Optimization of NK CRISPR screens.**

518 A) Western blot showing spCas9 expression in clonal isolates of K562 cells infected with a
519 Cas9-expressing lentivirus. Asterisk highlights the clone used for screening purposes.

520 B) Measurement of Cas9 activity using an EGFP disruption assay. Cas9-expressing K562
521 cells were infected at a low MOI with a lentivirus expressing EGFP and a sgRNA targeting
522 EGFP. The percent of cells that lost EGFP expression was measured over time by flow
523 cytometry.

524 C) Measurement of Cas9 activity using sgRNAs targeting mismatch-repair (MMR) complex
525 members. A Cas9-expressing K562 clonal isolate was infected at a low MOI with a
526 lentivirus expressing sgRNAs against core members of the MMR complex. Protein
527 disruption was measured by western blot 10 days after sgRNA infection. Note that certain
528 MMR complex members depend on other binding partners for stability.

529 D) Experimental design for determining selective pressure of different E:T cell ratios. K562
530 cells were labeled with carboxyfluorescein succinimidyl ester (CFSE) prior to co-culture
531 with NK-92 cells.

532 E) Effect of increasing E:T cell ratio on total number of viable target cells over time. During
533 early timepoints, CFSE fluorescence was used to generate target cell counts. At later
534 timepoints, total cell counts accurately reflected target cell counts due to NK-92 cell death.
535 F) Representative image of NK-92:K562 co-cultures at 5:1 E:T ratio. NK-92 cells (unlabeled)
536 form aggregate structures enveloping the target cells (green). Scale bar, 250μM.
537
538 **Figure 1 – figure supplement 2. Additional NK CRISPR screen data.**
539 A) Analysis of the NK CRISPR screen results performed at a lower E:T ratio. sgRNA
540 abundance was compared between the 1:1 E:T ratio co-culture condition and day 15
541 dropout cells using the MAGeCK algorithm. The computed false discovery rate (FDR) is
542 plotted against the -log10 transformation of the MAGeCK score. The top 5 enriched or
543 depleted genes are shown, as rank-ordered by MAGeCK score; other manually selected
544 genes are highlighted with their rank indicated in parentheses.
545
546 **Supplemental Table 1**. Design of genome-scale CRISPR library. sgRNA sequences and
547 coordinates of the intended target locus are provided.
548
549 **Supplemental Table 2**. NK CRISPR screen data. Normalized sgRNA counts and MAGeCK
550 analysis output are provided.
551
552 **Figure 2. A phenotypic screen based on MHC-I upregulation to identify modulators of the**
553 **IFNγ response**
554 A) Flow cytometry measurement of MHC-I expression in K562 cells transduced with the
555 indicated sgRNAs after 24hrs of 10ng/ml IFNγ treatment.
556 B) Fold upregulation of MHC-I expression after IFNγ treatment in K562 cells transduced with
557 the indicated sgRNAs. Mean and standard deviation are shown. *** P value= 0.0002, **
558 P value=0.03, Mann-Whitney test.
559 C) Design of CRISPR screen for IFNγ-induced upregulation of MHC-I expression. SSC, side-
560 scatter.
561 D) Analysis of the MHC-I upregulation CRISPR screen results. The MAGeCK algorithm was
562 used to compare sgRNA abundance between cells in the bottom two and top two deciles

563 of MHC-I expression. The false discovery rate (FDR) is plotted against the -log10
564 transformation of the MAGeCK score. The top 5 to 10 enriched or depleted genes are
565 shown, as rank-ordered by MAGeCK score; other manually selected genes are highlighted
566 with their rank indicated in parentheses.
567 E-F) Comparison of the NK and MHC screening results. Results of each screen were rank-
568 ordered based on their MAGeCK score. Select genes are highlighted.
569
570 **Figure 2 – figure supplement 1. Confirmation of gene disruption in K562 cells.**
571 A) Western blot of total STAT1 levels in K562 cells infected with control or STAT1 sgRNAs.
572 B) Western blot of PTPN2 levels in K562 cells infected with control or PTPN2 sgRNAs.
573
574 **Supplemental Table 3**. Raw MHC-I screen data. Normalized protospacer counts and MAGeCK
575 analysis output are included.
576
577 **Figure 3. Disruption of DCAF15 enhances NK effector functions**
578 A) Experimental design of competitive co-culture experiments, with FACS data illustrating a
579 hypothetical sgRNA that enhances NK-mediated target cell clearance.
580 B) Representative results from NK-92:K562 competitive co-culture experiments performed at
581 a 2.5:1 E:T ratio.
582 C) Results of competitive co-culture performed at a 2.5:1 E:T ratio and measured 48-96hrs
583 after challenge of K562 cells with NK-92 cells. Mean and standard deviation are shown.
584 *** P-value <0.0001, Mann-Whitney test.
585 D) Results of competitive co-culture performed at a 1:1 E:T ratio and measured 48-96hrs after
586 challenge of K562 cells with IL-2 activated isolated peripheral NK cells. ** P-value <0.01,
587 * P-value =0.06, Wilcoxon matched-pairs signed rank test.
588 E) Results of competitive co-culture performed at a 2.5:1 E:T ratio and measured 48-96hrs
589 after challenge of Daudi cells with NK-92 cells. Mean and standard deviation are shown.
590 *** P-value <0.0001, ** P-value=0.0022, * P-value=0.09, Mann-Whitney test.
591 F) Flow cytometry analysis of NK cell degranulation (cell surface CD107A expression) after
592 2hr coculture of primary NK cells with indicated target cell types at 2.5:1 E:T ratio. Line

593 indicates median value. ** P-value =0.095, * P-value=0.067, NS P-value>0.10, Mann-
594 Whitney test.
595
596 **Figure 3 – figure supplement 1. Confirmation of gene disruption in K562 and Daudi cells.**
597 A) Measurement of cell surface NECTIN2 expression by flow cytometry in K562 cells
598 expressing control or NECTIN2 sgRNAs. Gates show background levels of fluorescence.
599 B) Measurement of cell surface ICAM1 expression by flow cytometry in K562 cells
600 expressing control or ICAM1 sgRNAs. Gates show background levels of fluorescence.
601 C) Measurement of DCAF15 mRNA expression by RNAseq in K562 cells transduced with
602 control or DCAF15 sgRNAs.
603 D) Western blot of PTPN2 levels in Daudi cells infected with control or PTPN2 sgRNAs.
604 E) Measurement of cell surface ICAM1 expression by flow cytometry in Daudi cells
605 expressing control or ICAM1 sgRNAs. Gates show background levels of fluorescence.
606 F) Measurement of DCAF15 mRNA expression by RNAseq in Daudi cells transduced with
607 control or DCAF15 sgRNAs.
608
609 **Figure 3 – figure supplement 2. Co-culture of primary NK cells with K562 cells.**
610 A) Flow cytometry analysis of purity of isolated peripheral NK cells 24hrs after IL-2
611 stimulation.
612 B) Flow cytometry analysis of activation status of CD3-CD56+ NK cells after 24hrs of IL-2
613 stimulation.
614
615 **Figure 4. DCAF15 disruption leads to an inflamed state distinct from dysregulated IFNγ-**
616 **JAK-STAT signaling**
617 A) Flow cytometry measurement of cell surface MHC-I expression in K562 cells transduced
618 with the indicated sgRNAs after 24hrs of 10ng/ml IFNγ treatment. *** P <0.0001; ** P=
619 0.0044, Mann-Whitney test.
620 B) Western blots illustrating total and phosphorylated STAT1 after 30 minutes of 1ng/ml IFNγ
621 treatment in K562 cells infected with the indicated sgRNAs.

622 C) Growth rate of K562 cells expressing the indicated sgRNAs, cultured under basal
623 conditions ("untreated"), treated 24hrs with 10ng/ml IFNγ ("IFNγ pulse"), or continuously
624 retreated with 10ng/ml IFNγ every day ("IFNγ constant").
625 D) Principle component analysis (for principle components (PC) 1 and 3) of transcriptomes
626 from K562 cells expressing the indicated sgRNAs and treated +/- 10ng/ml IFNγ for 24hrs.
627 E) Selected GO terms, identified by RNA-seq, enriched in DCAF15 KO cells. Negative log10
628 transformation of the Benjamini-Hochberg corrected P value.
629 F) Volcano plot of genes differentially expressed between DCAF15 KO cells compared to
630 control KO cells. Selected genes are highlighted. The FDR-corrected P-value generated
631 from a likelihood ratio test (Q-value) is plotted against an approximate measure of the fold
632 change in expression (Beta value).
633
634 **Figure 4 – figure supplement 1**
635 A) Growth rate of K562 cells expressing sgRNAs against DCAF15 or a control gene. Results
636 from 2-3 independent experiments and 2-3 different sgRNAs per gene. Mean and standard
637 deviation are shown. DCAF15 sgRNAs, 1.1+/-0.01 population doublings per day. Control
638 sgRNAs, 1.13+/-0.03 population doublings per day.
639 B) Volcano plot of genes differentially expressed in control K562 cells after 24hrs of IFNγ
640 treatment. Selected genes are highlighted. Genes that were off-scale and could not be
641 plotted are shown in the oval. The FDR-corrected P-value generated from a likelihood ratio
642 test (Q-value) is plotted against an approximate measure of the fold change in expression
643 (Beta value).
644 C) Flow cytometry analysis of the change in cell surface expression of the indicated cell
645 surface markers in K562 cells transduced with the indicated sgRNAs after 24hrs of 10ng/ml
646 IFNγ treatment. ** P value= 0.003, * P value=0.026, Mann-Whitney test.
647 D) Gene set enrichment analysis (GSEA) of genes differentially upregulated in PTPN2 KO
648 cells. nES, normalized enrichment score. Categories with a FDR Q-value of <0.1 are
649 shaded in blue.
650 E) GSEA of genes differentially upregulated in PTPN2 KO cells after IFNγ treatment.
651

652 **Supplemental Table 4**. List of differentially expressed genes determined by RNA-seq of control,
653 DCAF15 or PTPN2 KO K562 cells.
654
655 **Figure 5. DCAF15 knockout cells enhance NK-92 triggering via CD80 expression**
656 A) Flow cytometry measurements of the indicated cell surface markers in K562 cells
657 expressing the indicated sgRNAs. N=9-24 samples per condition. *** P<0.0001, **
658 P=0.001, ns P>0.1, Mann-Whitney Test.
659 B) Flow cytometry measurement of CD80 surface expression in control K562 cells or those
660 transduced with lentivirus to overexpress CD80. Gate shows level of background
661 fluorescence in unstained cells.
662 C) Results of competitive co-culture between indicated K562 cell types and NK-92 cells,
663 performed at 1:1 E:T ratio. K562 cells were unmanipulated ("control") or overexpressed
664 wild-type CD80 ($CD80^{wt}$) or mutant CD80 ($CD80^{mut}$; contains Q65A and M72A point
665 mutations that abrogate CD28 binding). * P=0.005, ** P=0.0007, NS P>0.1, unpaired T
666 test.
667 D) Experimental design of CD80 blockade experiment.
668 E) Effect of blocking antibodies to CD80 on NK-92 activation, measured by CD107 flow
669 cytometry on NK-92 cells after 4hrs of co-culture. Data points from experiments performed
670 on the same day are joined by lines of the same color. ** P=0.03, * P=0.06, ns P>0.1,
671 Wilcoxon matched-pairs signed rank test. Experiment performed 4 times, 2x sgRNAs per
672 condition.
673 F) Percent decrease in NK-92 degranulation after CD80 antibody treatment of indicated target
674 cells. Data points from experiments performed same day are joined by lines. Mean is
675 indicated. ** P=0.03, Wilcoxon matched-pairs signed rank test.
676
677 **Figure 5 – figure supplement 1**
678 A) Flow cytometry measurements of the indicated cell surface markers in K562 cells
679 expressing the indicated sgRNAs. N=2-14 samples per condition. Ns P>0.1, * P=0.04, **
680 P=0.01, Mann-Whitney Test.
681 B) Experimental design for rescuing DCAF15 disruption in K562 by lentiviral expression of
682 a sgRNA-resistant DCAF15 open reading frame.

683 C) Western blot of DCAF15 rescue construct expression.
684 D) Flow cytometry measurements of the indicated cell surface markers in K562 cells
685 expressing the indicated sgRNAs and rescue constructs. N=6-24 samples per condition.
686 *** P<0.0001, ** P=0.004, Mann-Whitney test.
687 E) Flow cytometry measurement of CTLA4 and CD28 expression on NK-92 cells. Gates show
688 background fluorescence levels in unstained cells.
689 F) Flow cytometry measurement of CD28 expression in peripheral unstimulated NK cells.
690
691 **Figure 6. The anti-leukemia drug indisulam inhibits DCAF15 function**
692 A) Proposed model for DCAF15 gain- and loss-of-function phenotypes triggered by indisulam
693 treatment.
694 B) Dose response of K562 cells expressing the indicated sgRNAs to indisulam. Relative
695 viability measured by ATP content. N=2 experiments. Mean and standard deviation are
696 shown.
697 C) Growth of K562 cells treated with 0.1μM indisulam over 4 days. N=12 per timepoint.
698 Mean and standard deviation are shown.
699 D) Western blot for total RBM39 levels in K562 cells after 0.1μM indisulam treatment for the
700 indicated number of days.
701 E) Flow cytometry measurements of the indicated cell surface markers in K562 cells after
702 indisulam treatment. Mean and standard deviation are shown. *** P<0.0001, ** P=0.0085,
703 * P=0.013, mean significantly different from 1, one sample T test.
704 F) CD80 expression measured by flow cytometry in indisulam-treated K562 cells expressing
705 the indicated sgRNAs. Mean and standard deviation are shown. N=4-6 samples. **
706 P=0.0095, * P=0.0286, ns P>0.1, Mann-Whitney test.
707 G) Effect of indisulam treatment on CD80 expression in the indicated cell lines. N=3-12
708 samples. Mean and standard deviation are shown. *** P<0.0001, ** P= 0.0066, mean
709 significantly different from 1, one sample T test.
710 H) Kaplan-Meier analysis of overall survival in adult AML patients from TCGA LAML
711 project stratified by DCAF15 expression. “DCAF15 high” and “DCAF15 low” represents
712 patients in top or bottom 50% of DCAF15 expression, respectively. N=142 patients. 95%

713 confidence interval shown. Median survival, 16.17 vs 12.18 months. P-value from log-rank
714 test.
715 I) Kaplan-Meier analysis of overall survival in pediatric AML patients from TARGET project
716 stratified by DCAF15 expression. "DCAF15 high" and "DCAF15 low" represents patients
717 in top or bottom 20% of DCAF15 expression, respectively. N=76 patients. 95% confidence
718 interval shown. Median survival, 21.17 vs NA. P-value from log-rank test.
719
720 **Figure 6 – figure supplement 1**
721 A) Relationship between DCAF15 mRNA expression and indisulam sensitivity across a panel
722 of cell lines.
723 B) Time-course of CD80 expression after indisulam treatment in K562 cells measured by flow
724 cytometry. Blue shading indicates period of CD80 upregulation. N=2-4 samples per
725 timepoint. Mean and standard deviation are shown.
726 C) CD80 expression measured by flow cytometry across a panel of cancer cell lines. Dashed
727 line indicates background level of antibody staining, with cell lines in red have expressing
728 above background levels of the protein. CML, chronic myelogenous leukemia. BL,
729 Burkitt's lymphoma. AML, acute myeloid leukemia. AMoL, acute monocytic leukemia.
730 T-ALL, T-acute lymphoblastic leukemia. MM, multiple myeloma. ALCL, anaplastic large
731 cell lymphoma.
732 D) Growth of Daudi and KU812 cells treated with 0.1μM indisulam over 4 days. N=3 per
733 timepoint. Mean and standard deviation are shown.
734 E) Fold change in CD80 expression in the indicated cell lines after 4 days treatment with
735 0.1μM indisulam.
736 F) Box and whisker plot of DCAF15 expression in TCGA LAML samples, stratified by
737 subtype using the French American British (FAB) AML classification scheme. Analysis
738 from UALCAN portal [61]. Subtypes with significantly different median expression values
739 are indicated.
740 G) FAB classification of adult AML patients in the TCGA LAML project, stratified by top
741 50% ("DCAF15 high") or bottom 50% ("DCAF15 low") of DCAF15 expression.
742
743 **Figure 7. Cohesin complex members are CRL4-DCAF15 E3 ligase client proteins**

744

745 A) Experimental system for discovering DCAF15 interaction partners by proximity ligation.

746 B) Indicated constructs were stably expressed in K562 cells, and biotinylated proteins detected
747 by HRP-conjugated streptavidin ("α-biotin"). Asterisks denote major endogenous biotin-
748 containing proteins. "MG132" and "Biotin" refer to 18hrs treatment with 5μM MG132 or
749 50μM biotin.

750 C) Proteins identified by quantitative mass spectrometry as differentially biotinylated by
751 DCAF15-BioID as compared to GFP-BioID. Log2-fold changes are plotted against
752 precision of the measurement (1/ coefficient of variation). Colors denote the posterior
753 probability that a protein fold change was small (referred to as "P-null" in the legend), as
754 explained in the methods. Data points in red are select CRL4 core complex members. Data
755 points in blue are endogenous biotin-containing proteins.

756 D-E) Affinity capture of biotinylated proteins by streptavidin beads ("biotin IP") and detection
757 by western blot. Indicated constructs were stably expressed in K562 cells. "Indisulam"
758 refers to 48hrs 0.1μM indisulam treatment prior to MG132 and biotin addition.

759 F) Capture of 6xhis-ubiquitinated species by nickel chromatography under denaturing
760 conditions and detection by western blot. The indicated expression plasmids were
761 transiently transfected into 293T cells. Input samples were prepared from whole cell lysates
762 (WCL). "MG132" and "Indisulam" refer to 12hrs treatment with 10μM MG132 or 2μM
763 Indisulam prior to harvest.

764 G) Model of DCAF15 function.

765

766 **Figure 7 – figure supplement 1**

767 A) Exogenous DCAF15 interacts with CRL4 core complex members. Indicated constructs
768 were stably expressed in K562 cells. Anti-Flag immunoprecipitations were performed and
769 analyzed by western blot.

770

771 **Supplemental Table 5.** Comparison of biotinylated proteins recovered from K562 cells
772 expressing DCAF15-BIoID or GFP-BioID using isobaric labeling and mass spectrometry.

773

774 **Supplemental Table 6.** List of sgRNA sequences used.

775

776 **Supplemental Table 7.** List of antibodies used.

777

778 **Supplemental Table 8.** Primer design for sequencing sgRNA libraries.

779

780

781 **Materials and methods**

782

783 ***Cell lines***

784 All cell lines were purchased from ATCC and were tested monthly for mycoplasma contamination.
785 Cell lines other than NK-92 were maintained in RPMI supplemented with 10% FBS, 1mM
786 GlutaMAX and 1% antibiotic, antimycotic. NK-92 cells were grown in Myelocult H5100 (Stem
787 cell Technologies) supplemented with 100U/ml human IL-2 (Peprotech cat#200-02). IL-2 stock
788 solution was made by reconstituting lyophilized cytokine to 10e6 U/ml in 50mM acetic acid, 0.1%
789 BSA in PBS.

790

791 ***Construction of the CRISPR Library***

792 CRISPR screening was performed using bespoke genome-scale libraries, to be described in detail
793 elsewhere. In brief, the sgRNA library was designed with 120,021 sgRNAs present, representing
794 6 guides each against 21,598 genes and 4 guides each against 1,918 miRNAs, as well as 1000 non-
795 targeting negative control guides (Table S1). sgRNAs targeting protein-coding genes were based
796 on the Avana libraries [62]. sgRNAs targeting miRNAs were based on the design of the Gecko v2.0
797 libraries [63]. The protospacer library was synthesized by Twist Biosciences. The synthesized oligo
798 library was amplified using emulsion PCR followed by purification. The vaccinia virus DNA
799 polymerase was used to clone the protospacers into a lentiviral construct (In-fusion, Takara). The
800 lentiviral construct was linearized by Bfua1 digestion (New England Biolabs). To ensure complete
801 digestion, Bfua1 activity was stimulated by addition of 500nM of a double-stranded oligo
802 containing a Bfua1 site (5' atagcacctgctata 3') (based on [64]).

803

804 The guide RNAs were expressed from a human U6 promoter, using a modified sgRNA design (A-
805 U flip, longer stem-loop) previously described [65]. An EF1a-Puro-T2A-cerulean-wpre ORF was
806 used for selection purposes and for measuring infection rates. The library was electroporated into
807 MegaX cells and plated across 37x 500cm^2 LB-carbenicillin plates. The library was recovered and
808 pooled by scraping and column-based plasmid purification (Zymopure GigaPrep).

809

810 ***Preparation of virions***

811 16M 293T cells were plated onto 177cm^2 dishes (9x plates total). 24hrs later, cell media was
812 replaced with 32mls of DMEM+10% FBS (D-10). Cells were transfected with the library by
813 lipofection (per plate: 158ul lipofectamine 2000, 8mls of Optimem, 3.95µg of VSVG, 11.8µg of
814 Pax2, 15.78µg of library). The transfection mixture was left on the cells overnight, then changed
815 to 25mls of D-10. Viral supernatant was collected 48hrs later. Debris was removed by
816 centrifugation at 200g. Aliquots were flash-frozen and stored at -80°C.
817
818 ***Validation of the Cas9-expressing cell line used for screening***
819 K562 cells were lentivirally infected with an EF1a-spCas9-T2A-blastR construct. Following
820 10µg/ml blasticidin selection, cells were dilution cloned. Clonal isolates with high levels of cas9
821 expression (as determined by western blot) were selected for further characterization. To determine
822 the kinetics and efficacy of gene cutting under screening conditions (*e.g.*, low multiplicity of
823 infection (MOI)) of the sgRNA construct), cells were infected with a lentiviral construct
824 expressing both EGFP and a sgRNA targeting GFP. Following puromycin selection, the loss of
825 EGFP expression was monitored by flow cytometry. In other experiments, the ability to effectively
826 deplete endogenous proteins was determined by using a series of sgRNAs targeting the mismatch
827 repair complex and measuring protein depletion by western blot.
828
829 ***NK screen***
830 Five hundred million spCas9-expressing K562 cells were mixed with CRISPR sgRNA library
831 virions and 1L of media, then distributed across 34 6-well plates. Cells were spin-infected at 1900
832 rpm for 30 min at room-temperature with CRISPR library virus, conditions calculated to achieve
833 a MOI of ~0.3 and 1000 cells per sgRNA library representation. MOI was measured by tracking
834 the percent of the population expressing the cerulean marker found in the sgRNA library. Cells
835 were incubated overnight in viral supernatant prior to being pooled, spun down to remove virions,
836 and returned to spinner-flask culture (Bell-Flo Flask, Bellco Glass Inc). 24 to 48hrs post-infection,
837 2µg/ml puromycin selection was started for four days. Cells were maintained in log-growth phase
838 with a minimal representation of 500M cells. Seven days post guide-infection, NK cell challenge
839 was initiated. For the 2.5:1 E:T challenge, 100M K562 cells were mixed with 250M NK-92 cells
840 in 1L of Myelocult, and split across 25 177cm^2 dishes. For the 1:1 E:T challenge, 100M K562 cells
841 were mixed with 100M NK-92 cells in 400mls of Myelocult, and split across 10 177cm^2 dishes.

842 As a control, K562 cells were continuously propagated in RPMI media. 2 days after initiating the
843 NK-92 challenge, the co-culture was switched to RPMI media. NK-92 cells, when grown in RPMI
844 without IL-2, are rapidly lost from the culture. Six days after the media switch, 100M cell pellets
845 were generated for library construction. All cell pellets were stored cryopreserved in cell-freezing
846 media (Gibco #12648).
847
848 ***MHC-I screen***
849 Generation of K562 cells expressing the sgRNA library was performed as described above. On
850 day 8 post-guide infection, 150M cells were stimulated with 10ng/ml IFNγ (R&D Systems 285-
851 IF). 24hrs later, cells were spun down, washed, and stained in 3mls of 1:200 anti-HLA ABC-APC
852 (W6/32 clone, BioLegend) in PBS, 2% FBS for 30min at 4°c. Approximately 10M of the brightest
853 20% and dimmest 20% of cells were sorted (BD FACSAria Fusion). Cell purity was determined
854 to be >95% by re-analysis post-sorting. A replicate of this experiment was performed on day 14
855 post-guide infection.
856
857 ***CRISPR library preparation and sequencing***
858 Genomic DNA was prepared by thawing cryopreserved cell pellets and proceeding with DNA
859 extraction using column-based purification methods (NucleoSpin Blood XL, Machery-Nagel).
860 Protospacer libraries were generated by a two-step PCR strategy, modified from [66]. In the first
861 round of PCR, 150µg of gDNA (equivalent to 15M K562 cells and 125-fold coverage of the
862 library) was used in a 7.5ml PCR reaction to amplify the protospacers. This reaction was performed
863 using a 500nM mixture of primers containing 0-9bp staggers, to ensure base-pair diversity during
864 Illumina sequencing (see supplemental table S7). The reaction was performed with Phusion master
865 mix (New England Biolabs) and 3% DMSO with the following cycling conditions: 1 cycle X 30 s
866 at 98°C, 21 cycles X 15 s at 98°C, 20 s at 63°C, 15 s at 72°C, 1 cycle X 2 min at 72°C. In the
867 second round of PCR, 4µl of the initial PCR product was used as the template in a 200µl PCR
868 reaction to make the sample compatible with Illumina chemistry and to add unique I5 and I7
869 barcodes to the sample. The reaction was performed with Phusion master mix (New England
870 Biolabs), 500nM primers and 3% DMSO with the following cycling conditions: 1 cycle X 30 sec
871 at 98°C, 12 cycles X 15 s 98°C, 20 s at 60°C, 15 s at 72°C, 1 cycle X 2 min at 72°C. The library
872 was size-selected first by a 1:1 SPRI bead selection (AMPure XP beads, Beckman Coulter),

873 quantified by high-sensitivity dsDNA Qubit (ThermoFisher Scientific), and pooled. An agarose
874 size selection step (PippinHT, Sage Science) was performed prior to sequencing on an Illumina
875 Hiseq4000.
876
877 ***Screen analysis***
878 Libraries were sequenced to a depth of ~20 million reads per condition. Reads were aligned to the
879 sgRNA library using bowtie2. Protospacer count tables were generated from these alignments with
880 python scripts and processed with MAGeCK. MAGeCK analysis was used to score and prioritize
881 sgRNAs, using default settings in the algorithm [23]. A subset of genes, mostly from highly related
882 gene families, have more than 6 sgRNAs targeting them. As the MAGeCK scoring method tends
883 to prioritize consistency of effect over magnitude of effect, genes with more than 6 guides targeting
884 them were excluded from the analysis. MAGeCK scores were -log10 normalized, and values were
885 plotted against FDR values.
886
887 ***NK-92 competitive co-culture assay***
888 Cas9-expressing K562 or Daudi cells were transduced at a high MOI with a lentiviral sgRNA
889 construct expressing the guide of interest, puromycin resistance and CMV promoter-driven
890 expression of either a red or green fluorescent protein. Knockout cell populations were maintained
891 in a polyclonal state. Gene disruption was confirmed at the protein level by flow cytometry or
892 western blot, and by RNA-seq when antibody reagents were not available. Complete knockout in
893 >90% of the population was routinely achieved (Figure 2 – figure supplement 1 and Figure 3-
894 figure supplement 1). Cells were counted and 0.25M red-labeled test cells were mixed with 0.25M
895 green-labeled control cells (expressing a sgRNA against an olfactory receptor gene). The mixture
896 was either grown in RPMI or mixed with 1.25M NK-92 cells in 4mls Myelocult media in 6-well
897 plates. The ratio of green-to-red cells was measured 2 to 4 days post-challenge, with the fold-
898 change normalized to the ratio in the non-challenged state (to control for differences in basal cell
899 growth rate).
900
901 ***Primary NK cell isolation***
902 PBMCs were isolated from leukocyte-enriched blood of human donors (Stanford Blood Center).
903 Donors were not genotyped or pre-screened for infectious disease markers. Natural killer cells

904 were isolated by negative selection using magnetic columns (Miltenyi 130-092-657). Purity post-
905 selection was routinely >97% CD56+ CD3-. Isolated NK cells were plated at 1M/ml density in
906 96-well u-bottom plates and stimulated overnight with 1000U/ml IL-2 in complete RPMI with
907 10% FBS.
908
909 ***Primary NK cell degranulation assay***
910 Following IL-2 activation, NK cells were counted and mixed with target cells in 96-well u-bottom
911 plates. 100,000 NK cells were mixed with 40,000 target cells in a final volume of 200µl for a 2.5:1
912 E:T ratio. Cells were co-cultured at 37°C for 2 hrs, then stained with anti-CD56-BV421 (1:200)
913 and anti-CD107a-APC (1:200 dilution) for 30m at 4°C. CD107a expression was assayed by flow
914 cytometry in the 7-AAD- CD56+ RFP- GFP- cell population. Primary NK cells exhibited very
915 little basal degranulation in the absence of target cells (<1% CD107a+). The assay was repeated
916 with 6 primary donors with technical duplicates.
917
918 ***Primary NK cell competitive co-culture assay***
919 Following IL-2 activation, NK cells were counted and mixed at a 1:1 E:T ratio with RFP-labeled
920 target cells and GFP-labeled control cells in a 96-well u-bottom plate. 50,000 NK cells were
921 combined with 25,000 Red and 25,000 Green cells in a final volume of 200µl and continuously
922 expanded in 96-well plates to as needed. The ratio of GFP+ to RFP+ cells was measured by flow
923 cytometry on days 2 and 4 post-challenge, and the fold change was normalized to the ratio in the
924 non-challenged state (to control for differences in basal cell growth rate). The assay was repeated
925 with 6 primary donors with technical duplicates.
926
927 ***Flow cytometry***
928 0.5 to 1M cells were spun down and stained with APC-conjugated antibodies for 30mins at 4°c in
929 PBS with 2% FBS. Cells were analyzed on a BD LSRFortessa. The geometric mean fluorescence
930 intensity of singlet, DAPI-excluding cells was measured, and normalized to the background
931 fluorescence of that particular genotype of cells.
932
933 ***DCAF15 rescue experiments***

934 The DCAF15 open reading frame was synthesized based off reference sequence NM_138353, but
935 with silent mutations designed to confer resistance to all three sgRNAs. To ensure resistance to
936 sgRNA-directed gene cutting, silent mutations were introduced to the PAM domain and the
937 proximal region of the protospacer (guide #1: 5' GCTGCACACCAAGTACCAGGTGG to
938 GCTGCACACCAAaTAtCAaGTaG. Guide #2: 5' TGACATCTACGTCAGCACCGTGG to
939 TGACATCTACGTCtcCACaGTaG; Guide #3: 3' GCAGCTTCCGGAAGAGGCGAGGG to
940 GCAGCTTCCGGAAtaaaCGtGGt).
941
942 The rescue construct was expressed lentivirally from an EF1a promoter, with a c-terminal 3-flag
943 epitope tag. Rescue cells were selected with hygromycin. The rescue construct was introduced two
944 weeks after the initial introduction of the DCAF15 sgRNAs, and stable cell lines generated by a
945 week of selection in 375μg/ml hygromycin. Expression of the construct was confirmed by lysing
946 cells in PBS+0.1% NP40 (as per [49]) and western blotting for the Flag tag.
947
948 ***CD80 blocking experiments***
949 RFP-labeled target cells (0, 0.75M, or 2.5M) were resuspended in 0.5mls Myelocult + 5μg/ml
950 control (MOPC-21 clone) or blocking CD80 (2D10 clone) antibodies. Cells were incubated for 30
951 mins at room temperature. 0.5M NK-92 cells in 0.5mls Myelocult were added to the well with
952 1:200 anti-CD107a-APC antibody. Cells were co-cultured for 4hrs at 37°C. Flow cytometry was
953 used to measure CD107A-APC expression in the NK-92 (RFP-negative) population. NK-92 cells
954 were found to display a basal level of CD107a expression in the absence of effector cells. Increases
955 above basal staining levels were used to define NK-92 degranulation. The experiment was repeated
956 4 times to establish biological replicates.
957
958 ***CD80 over-expression experiments***
959 A full-length CD80 open reading frame, based on reference sequence NM_005191.4, was
960 synthesized with a c-terminal 3x Flag tag and expressed lentivirally from the EF1a promoter. Over-
961 expressing cells were selected with hygromycin. As a control construct, a mutant version of CD80
962 was synthesized with Q65A and M72A mutations in the "V-type" Ig-like domain. Each of these
963 residues makes contacts with CTLA4 in published CD80-CTLA4 co-crystal structures [67] and

964 alanine scanning experiments have shown that these residues are required for CD80 binding to
965 CD28 or CTLA4 [47].
966
967 ***sgRNA sequences used***
968 See supplemental table 6.
969
970 ***Antibodies used***
971 See supplemental table 8.
972
973 ***Cell viability after in vitro cytokine stimulation***
974 Cells were plated at 0.25M/ml in media with or without 10ng/ml IFNγ. Every day, an aliquot of
975 cells was counted (Vi-CELL XR, Beckman Coulter), and cells were diluted in fresh media to
976 maintain them in logarithmic growth phase. Continuously-treated cells were re-fed with fresh
977 10ng/ml IFNγ every day, whereas pulse-treated cells only received 24hrs of cytokine treatment.
978
979 ***Western Blotting***
980 Cells were counted, spun down and washed in PBS prior to lysis in NP40 lysis buffer (25mM
981 HEPES pH 7.5, 150mM NaCl, 1.5mM $MgCl_2$, 0.5% NP40, 10% glycerol, 2mM DTT) with
982 protease and phosphatase inhibitors. Lysates were normalized by cell count and/or protein
983 concentration. 20-40μg of lysates were used for western blot analysis using standard procedures.
984 Antibody binding was detected by enhanced chemiluminescence (SuperSignal Dura, Thermo
985 Scientific).
986
987 ***RNA-sequencing analysis***
988 Cells were seeded at 0.33M/ml density. Twenty-four hours later, 2M cells were collected. RNA
989 was first purified by TRizol extraction and then further purified using column-based methods and
990 polyA selection. RNAseq libraries were constructed using TruSeq Stranded mRNA Library Prep
991 Kits (Illumina) and were sequenced on an Illumina Hiseq4000 machine using 150bp paired-end
992 reads. Transcript abundances were quantified using Salmon (v0.9.1) in pseudo-alignment mode,
993 without adapter trimming, using the Ensembl GRCh38 transcriptome [68]. Differential expression
994 analysis was performed using Sleuth (v0.29.0) [69]. RNA-seq analysis was executed and visualized

995 using an in-house web-based platform. RNA sequencing data is available under accession number
996 GEO:GSE134173.
997
998 ***Indisulam treatment***
999 Indisulam (Sigma SML1225) was reconstituted at 10mM in DMSO and stored in single use
1000 aliquots at -80°C. For indisulam dose-response experiments, 5000 cells were plated in 384-well
1001 plates (Greiner) and treated with indisulam over a 72hr period. A 12-point dose-response was
1002 performed between 10μM and 4.9μM of drug, as dispensed by a Tecan D300e. Cell viability was
1003 measured by ATP quantification (Cell Titer Glo, Promega). Dose-response measurements were
1004 fitted to a sigmoidal curve and an IC50 determined (Prism, GraphPad Software). DCAF15
1005 expression data from different cell lines was downloaded from the Cancer Cell Line Encyclopedia
1006 [70] (https://portals.broadinstitute.org/ccle)
1007
1008 For low-dose indisulam experiments, cells were plated at 0.4M/ml in media with or without 100nM
1009 indisulam (1:100,000 dilution of stock). Cells were diluted every day in fresh media and drug to
1010 maintain them in logarithmic growth phase. Cells were analyzed for CD80 expression 96hrs after
1011 initiation of treatment.
1012
1013 ***AML survival analysis***
1014 FPKM RNAseq quantification for patient samples from the TARGET and TCGA LAML cohorts
1015 was obtained from the NIH NCI Genomic Data Commons DATA portal
1016 (https://portal.gdc.cancer.gov/). Clinical data for that TARGET AML and TCGA LAML cohorts
1017 were obtained from the Genomic Data Commons DATA portal and the Broad Institute TCGA
1018 Genome Data Analysis Center (http://gdac.broadinstitute.org/) respectively. Patients with
1019 matching clinical and transcript abundance data patients were stratified by DCAF15 expression as
1020 indicated. Survival time and vital status were defined as 'Overall Survival Time in Days' and 'Vital
1021 Status' respectively for the Target AML cohort. For the TCGA LAML study survival time for
1022 deceased patients ('patient.vital_status'=dead) was defined as 'patient.days_to_death' while for
1023 living patients ('patient.vital_status'=alive) 'patient.days_to_last_followup' was used for survival
1024 time. Survival analysis and Kaplan–Meier plots were generated using lifelines software for python
1025 (https://doi.org/10.5281/zenodo.2584900).

1026

1027 ***DCAF15 proximity ligation***

1028 K562 cells were infected with lentivirus expressing DCAF15-3flag-BioID-HA-T2A-BlastR,
1029 DCAF16-3flag-BioID-HA-T2A-BlastR, or 3flag-GFP-T2A-BioID-HA-T2A-BlastR. Stable cell
1030 lines were generated by 10μg/ml blasticidin selection. In triplicate, 20M cells were grown in media
1031 supplemented with 50μm biotin and 5μm MG132. 18hrs later, cell pellets were washed three times
1032 with ice cold PBS and lysed in mild lysis buffer (PBS 0.1% NP40 + PI/PPI), conditions determined
1033 to maximize the solubility of over-expressed DCAF15. 1mg of clarified lysate was used for
1034 enrichment of biotinylated species. Lysates were mixed with 60ul of streptavidin beads (Pierce
1035 #88817) for 4hrs at 4°c in 500μl total volume. Beads were collected on a magnetic column, washed
1036 twice with 1ml RIPA buffer (25mM HEPES-KOH pH 7.4, 150mM NaCl, 1% Triton X-100, 0.5%
1037 sodium deoxycholate, 0.1% SDS, 1mM EDTA) and three times with 1ml urea buffer (2M urea,
1038 10mM TRIS-HCl pH 8.0).

1039

1040 For western blotting experiments, after urea washing, beads were equilibrated in mild lysis buffer.
1041 Elution was performed by incubating the beads 15min at 23°C, 15min at 95°C in 30μl 2.5X
1042 Laemlli buffer supplemented with 10mM biotin and 20mM DTT. The eluate was brought down to
1043 1X concentration with lysis buffer prior to western blotting. We note that detection of total
1044 biotinylated species by western blot was extremely sensitive to detection conditions. Membranes
1045 were blocked for 10min in PBS, 2.5%BSA, 0.4% Triton-X 100. 1ng/ml streptavidin-HRP in
1046 blocking buffer was added for 25min at room temperature. The membrane was washed for 15min
1047 in PBS 0.4% TritonX-100 prior to ECL exposure.

1048

1049 To measure BioID activity after indisulam treatment, cells were treated for 48hrs with 0.1μm
1050 indisulam, followed by 24hrs in indisulam with 50μm biotin and 5μm MG132.

1051

1052 ***Proteomic analysis of DCAF15 interaction partners***

1053 For proteomics experiments, after the urea buffer washes, the samples were resuspended in
1054 denaturing buffer (8M urea, 50 mM ammonium bicarbonate pH 7.8). Proteins were reduced with
1055 dithiothreitol (5 mM, RT, 30min) and alkylated with iodoacetamide (15 mM RT, 45 min in the
1056 dark). Excess iodoacetamide was quenched with dithiothreitol (5 mM, room temperature, 20 min

1057 in the dark). The samples were diluted to 1 M urea using 50 mM ammonium bicarbonate and then
1058 digested with trypsin (37°C, 16h). After protein digestion, samples were acidified with
1059 trifluoroacetic acid to a final concentration of 0.5% and desalted using C18 StageTips [71]. Peptides
1060 were eluted with 40% acetonitrile/5% formic acid then 80% acetonitrile/5% formic acid and dried
1061 overnight under vacuum at 25°C (Labconco CentriVap Benchtop Vacuum Concentrator, Kansas
1062 City, Mo).
1063
1064 For tandem mass tag (TMT) labeling, dried peptides were resuspended in 50µL 200mM
1065 HEPES/30% anhydrous acetonitrile. TMT reagents (5 mg) were dissolved in anhydrous
1066 acetonitrile (250µL) of which 10µL was added to peptides to achieve a final acetonitrile
1067 concentration of approximately 30% (v/v). Following incubation at room temperature for 1 h, the
1068 reaction was quenched with 5% hydroxylamine/200mM HEPES to a final concentration of 0.3%
1069 (v/v). The TMT labeled peptides were acidified with 50µL 1% trifluoroacetic acid and pooled prior
1070 to desalting with SepPak (Waters) and dried under vacuum.
1071
1072 The pooled TMT-labeled peptides were fractionated using high pH RP-HPLC. The samples were
1073 resuspended in 5% formic acid/5% acetonitrile and fractionated over a ZORBAX extended C18
1074 column (Agilent, 5µm particles, 4.6 mm ID and 250 mm in length). Peptides were separated on a
1075 75-min linear gradient from 5% to 35% acetonitrile in 10mM ammonium bicarbonate at a flow
1076 rate of 0.5mL/min on an Agilent 1260 Infinity pump equipped with a degasser and a diode array
1077 detector (set at 214, 220, and 254nm wavelength) from Agilent Technologies (Waldbronn,
1078 Germany). The samples were fractionated into a total of 96 fractions and then consolidated into 12
1079 as described previously [72]. Samples were dried down under vacuum and reconstituted in 4%
1080 acetonitrile/5% formic acid for LC-MS/MS processing.
1081
1082 Peptides were analyzed on an Orbitrap Fusion Lumos mass spectrometer (Thermo Fisher
1083 Scientific) coupled to an Easy-nLC (Thermo Fisher Scientific). Peptides were separated on a
1084 microcapillary column (100 µm internal diameter, 25 cm long, filled using Maccel C18 AQ resin,
1085 1.8µm, 120A; Sepax Technologies). The total LC-MS run length for each sample was 180 min
1086 comprising a 165 min gradient from 6 to 30% acetonitrile in 0.125% formic acid. The flow rate
1087 was 300 nL/min and the column was heated to 60°C.

1088

1089 Data-dependent acquisition (DDA) mode was used for mass spectrometry data collection. A high
1090 resolution MS1 scan in the Orbitrap (m/z range 500-1,200, 60k resolution, AGC 5 x 10^5, max
1091 injection time 100 ms, RF for S-lens 30) was collected from which the top 10 precursors were
1092 selected for MS2 analysis followed by MS3 analysis. For MS2 spectra, ions were isolated using a
1093 0.5 m/z window using the mass filter. The MS2 scan was performed in the quadrupole ion trap
1094 (CID, AGC 1 x 10^4, normalized collision energy 30%, max injection time 35 ms) and the MS3
1095 scan was analyzed in the Orbitrap (HCD, 60k resolution, max AGC 5x10^4, max injection time
1096 250 ms, normalized collision energy 50). For TMT reporter ion quantification, up to six fragment
1097 ions from each MS2 spectrum were selected for MS3 analysis using synchronous precursor
1098 selection (SPS).

1099

1100 Mass spectrometry data were processed using an in-house software pipeline [73]. Raw files were
1101 converted to mzXML files and searched against a composite human uniprot database (downloaded
1102 on 29th March 2017) containing sequences in forward and reverse orientations using the Sequest
1103 algorithm. Database searching matched MS/MS spectra with fully tryptic peptides from this
1104 composite dataset with a precursor ion tolerance of 20 ppm and a product ion tolerance of 0.6 Da.
1105 Carbamidomethylation of cysteine residues (+57.02146 Da) and TMT tags of peptide N-termini
1106 (+229.162932 Da) were set as static modifications. Oxidation of methionines (+15.99492 Da) was
1107 set as a variable modification. Linear discriminant analysis was used to filter peptide spectral
1108 matches to a 1 % FDR (false discovery rate) as described previously [73]. Non-unique peptides that
1109 matched to multiple proteins were assigned to proteins that contained the largest number of
1110 matched redundant peptides sequences using the principle of Occam's razor [73].

1111

1112 Quantification of TMT reporter ion intensities was performed by extracting the most intense ion
1113 within a 0.003 m/z window at the predicted m/z value for each reporter ion. TMT spectra were
1114 used for quantification when the sum of the signal-to-noise for all the reporter ions was greater
1115 than 200 and the isolation specificity was greater than 0.75 [74].

1116

1117 Base 2 logarithm of protein fold-changes were estimated by fitting a previously described Bayesian
1118 model [75] to the peptide level intensities. Protein estimates are reported as the mean of the posterior

1119 distribution for each parameter. Similarly, coefficients of variation are calculated by taking the
1120 posterior variance divided by the posterior mean. The probability of a small change ("P_null") was
1121 estimated as the frequency of posterior samples that fall within the interval (-1,1) on the log2 scale.
1122
1123 ***Polyubiquitination assay***
1124 Experiments were performed as per [76]. One million 293Ts were plated in 6-well dishes overnight.
1125 Cells were transfected with 500ng of plasmids containing CMV-6his-ubiquitin, CMV-3fl-EGFP,
1126 EF1A-DCAF15-3fl and/or CMV-SMC1A-HA. The SMC1A open reading frame was synthesized
1127 based on reference sequence NM_006306.3. After 36hrs, cells were treated with 2μM indisulam
1128 and/or 10μM MG132. 12hrs later, replicate wells were harvested for whole-cell lysates or for Ni-
1129 NTA pulldowns. Whole-cell lysates were made by extraction in 500μl NP40 lysis buffer. For Ni-
1130 NTA pulldowns, cells were solubilized in 700μl of guanidine buffer (6M guanidine-HCL, 0.1M
1131 Na_2HPO_4/NaH_2PO_4, 10mM imidazole, 0.05% TWEEN 20, pH 8.0), run through QIAshredder
1132 columns (Qiagen) and briefly sonicated. Purifications of 6his-ubiquinated species were performed
1133 as described in [76], except for the use of magnetic Ni-NTA beads (Thermo Fisher Scientific 88831)
1134 and the addition of 0.05% TWEEN 20 to wash buffers.
1135
1136 ***Data processing***
1137 Unless otherwise specified, data was graphed and statistically analyzed using Prism (GraphPad
1138 Software). Sample size was not predetermined, No outliers were excluded. Unless otherwise noted,
1139 all data points represent biological replicates rather than technical replicates. We define 'technical
1140 replicates' as running an assay multiple times on the exact same sample.
1141
1142 **Acknowledgements**
1143 We thank Jonathan Paw for flow cytometry and cell sorting; Margaret Roy, Andrea Ireland,
1144 Twaritha Vijay, Nicole Fong for next-generation sequencing; Adam Baker and Matt Sooknah for
1145 RNA-seq data visualization; Hugo Hilton, David Stokoe, and Robert Cohen for critical reading of
1146 the manuscript, and members of the Calico Oncology group for helpful discussion.
1147
1148 **Competing Interests**
1149 All authors are employees of Calico Life Sciences, LLC.

1150

1151 **References**

1152

1153 1 Snyder, A. *et al.* Genetic basis for clinical response to CTLA-4 blockade in melanoma. *N*
1154 *Engl J Med* **371**, 2189-2199, doi:10.1056/NEJMoa1406498 (2014).
1155 2 Tumeh, P. C. *et al.* PD-1 blockade induces responses by inhibiting adaptive immune
1156 resistance. *Nature* **515**, 568-571, doi:10.1038/nature13954 (2014).
1157 3 Mariathasan, S. *et al.* TGFbeta attenuates tumour response to PD-L1 blockade by
1158 contributing to exclusion of T cells. *Nature* **554**, 544-548, doi:10.1038/nature25501
1159 (2018).
1160 4 Galon, J. & Bruni, D. Approaches to treat immune hot, altered and cold tumours with
1161 combination immunotherapies. *Nat Rev Drug Discov*, doi:10.1038/s41573-018-0007-y
1162 (2019).
1163 5 Easwaran, H., Tsai, H. C. & Baylin, S. B. Cancer epigenetics: tumor heterogeneity,
1164 plasticity of stem-like states, and drug resistance. *Mol Cell* **54**, 716-727,
1165 doi:10.1016/j.molcel.2014.05.015 (2014).
1166 6 Zaretsky, J. M. *et al.* Mutations Associated with Acquired Resistance to PD-1 Blockade in
1167 Melanoma. *N Engl J Med* **375**, 819-829, doi:10.1056/NEJMoa1604958 (2016).
1168 7 Sade-Feldman, M. *et al.* Resistance to checkpoint blockade therapy through inactivation
1169 of antigen presentation. *Nat Commun* **8**, 1136, doi:10.1038/s41467-017-01062-w
1170 (2017).
1171 8 Kearney, C. J. *et al.* Tumor immune evasion arises through loss of TNF sensitivity. *Sci*
1172 *Immunol* **3**, doi:10.1126/sciimmunol.aar3451 (2018).
1173 9 Pan, D. *et al.* A major chromatin regulator determines resistance of tumor cells to T cell-
1174 mediated killing. *Science* **359**, 770-775, doi:10.1126/science.aao1710 (2018).
1175 10 Manguso, R. T. *et al.* In vivo CRISPR screening identifies Ptpn2 as a cancer
1176 immunotherapy target. *Nature* **547**, 413-418, doi:10.1038/nature23270 (2017).
1177 11 Patel, S. J. *et al.* Identification of essential genes for cancer immunotherapy. *Nature* **548**,
1178 537-542, doi:10.1038/nature23477 (2017).
1179 12 Dunn, G. P., Old, L. J. & Schreiber, R. D. The immunobiology of cancer
1180 immunosurveillance and immunoediting. *Immunity* **21**, 137-148,
1181 doi:10.1016/j.immuni.2004.07.017 (2004).
1182 13 Rodig, S. J. *et al.* MHC proteins confer differential sensitivity to CTLA-4 and PD-1
1183 blockade in untreated metastatic melanoma. *Sci Transl Med* **10**,
1184 doi:10.1126/scitranslmed.aar3342 (2018).
1185 14 Gao, J. *et al.* Loss of IFN-gamma Pathway Genes in Tumor Cells as a Mechanism of
1186 Resistance to Anti-CTLA-4 Therapy. *Cell* **167**, 397-404 e399,
1187 doi:10.1016/j.cell.2016.08.069 (2016).
1188 15 McGranahan, N. *et al.* Allele-Specific HLA Loss and Immune Escape in Lung Cancer
1189 Evolution. *Cell* **171**, 1259-1271 e1211, doi:10.1016/j.cell.2017.10.001 (2017).
1190 16 Marcus, A. *et al.* Recognition of tumors by the innate immune system and natural killer
1191 cells. *Adv Immunol* **122**, 91-128, doi:10.1016/B978-0-12-800267-4.00003-1 (2014).

1192 17 Moynihan, K. D. *et al.* Eradication of large established tumors in mice by combination
1193 immunotherapy that engages innate and adaptive immune responses. *Nat Med* **22**,
1194 1402-1410, doi:10.1038/nm.4200 (2016).
1195 18 Lopez-Soto, A., Gonzalez, S., Smyth, M. J. & Galluzzi, L. Control of Metastasis by NK Cells.
1196 *Cancer Cell* **32**, 135-154, doi:10.1016/j.ccell.2017.06.009 (2017).
1197 19 Chiossone, L., Dumas, P. Y., Vienne, M. & Vivier, E. Natural killer cells and other innate
1198 lymphoid cells in cancer. *Nat Rev Immunol* **18**, 671-688, doi:10.1038/s41577-018-0061-z
1199 (2018).
1200 20 Ljunggren, H. G. & Malmberg, K. J. Prospects for the use of NK cells in immunotherapy of
1201 human cancer. *Nat Rev Immunol* **7**, 329-339, doi:10.1038/nri2073 (2007).
1202 21 Klingemann, H. G. *et al.* Establishment and characterization of a human leukemic cell
1203 line (SR-91) with features suggestive of early hematopoietic progenitor cell origin. *Leuk*
1204 *Lymphoma* **12**, 463-470, doi:10.3109/10428199409073789 (1994).
1205 22 Maki, G., Klingemann, H. G., Martinson, J. A. & Tam, Y. K. Factors regulating the
1206 cytotoxic activity of the human natural killer cell line, NK-92. *J Hematother Stem Cell Res*
1207 **10**, 369-383, doi:10.1089/152581601750288975 (2001).
1208 23 Li, W. *et al.* MAGeCK enables robust identification of essential genes from genome-scale
1209 CRISPR/Cas9 knockout screens. *Genome Biol* **15**, 554, doi:10.1186/s13059-014-0554-4
1210 (2014).
1211 24 Brandt, C. S. *et al.* The B7 family member B7-H6 is a tumor cell ligand for the activating
1212 natural killer cell receptor NKp30 in humans. *J Exp Med* **206**, 1495-1503,
1213 doi:10.1084/jem.20090681 (2009).
1214 25 Selvaraj, P. *et al.* The T lymphocyte glycoprotein CD2 binds the cell surface ligand LFA-3.
1215 *Nature* **326**, 400-403, doi:10.1038/326400a0 (1987).
1216 26 Rolle, A. *et al.* CD2-CD58 interactions are pivotal for the activation and function of
1217 adaptive natural killer cells in human cytomegalovirus infection. *Eur J Immunol* **46**, 2420-
1218 2425, doi:10.1002/eji.201646492 (2016).
1219 27 Martin, M. *et al.* CD84 functions as a homophilic adhesion molecule and enhances IFN-
1220 gamma secretion: adhesion is mediated by Ig-like domain 1. *J Immunol* **167**, 3668-3676
1221 (2001).
1222 28 Veillette, A. Immune regulation by SLAM family receptors and SAP-related adaptors. *Nat*
1223 *Rev Immunol* **6**, 56-66, doi:10.1038/nri1761 (2006).
1224 29 Wang, N. *et al.* Cutting edge: The adapters EAT-2A and -2B are positive regulators of
1225 CD244- and CD84-dependent NK cell functions in the C57BL/6 mouse. *J Immunol* **185**,
1226 5683-5687, doi:10.4049/jimmunol.1001974 (2010).
1227 30 Stanietsky, N. *et al.* The interaction of TIGIT with PVR and PVRL2 inhibits human NK cell
1228 cytotoxicity. *Proc Natl Acad Sci U S A* **106**, 17858-17863, doi:10.1073/pnas.0903474106
1229 (2009).
1230 31 Bottino, C. *et al.* Identification of PVR (CD155) and Nectin-2 (CD112) as cell surface
1231 ligands for the human DNAM-1 (CD226) activating molecule. *J Exp Med* **198**, 557-567,
1232 doi:10.1084/jem.20030788 (2003).
1233 32 Jin, J., Arias, E. E., Chen, J., Harper, J. W. & Walter, J. C. A family of diverse Cul4-Ddb1-
1234 interacting proteins includes Cdt2, which is required for S phase destruction of the
1235 replication factor Cdt1. *Mol Cell* **23**, 709-721, doi:10.1016/j.molcel.2006.08.010 (2006).

1236 33 Jackson, S. & Xiong, Y. CRL4s: the CUL4-RING E3 ubiquitin ligases. *Trends Biochem Sci* **34**,
1237 562-570, doi:10.1016/j.tibs.2009.07.002 (2009).
1238 34 Uhlmann, F. SMC complexes: from DNA to chromosomes. *Nat Rev Mol Cell Biol* **17**, 399-
1239 412, doi:10.1038/nrm.2016.30 (2016).
1240 35 Mazumdar, C. & Majeti, R. The role of mutations in the cohesin complex in acute
1241 myeloid leukemia. *Int J Hematol* **105**, 31-36, doi:10.1007/s12185-016-2119-7 (2017).
1242 36 Chen, E., Karr, R. W., Frost, J. P., Gonwa, T. A. & Ginder, G. D. Gamma interferon and 5-
1243 azacytidine cause transcriptional elevation of class I major histocompatibility complex
1244 gene expression in K562 leukemia cells in the absence of differentiation. *Mol Cell Biol* **6**,
1245 1698-1705 (1986).
1246 37 Chen, L. & Flies, D. B. Molecular mechanisms of T cell co-stimulation and co-inhibition.
1247 *Nat Rev Immunol* **13**, 227-242, doi:10.1038/nri3405 (2013).
1248 38 Acuto, O. & Michel, F. CD28-mediated co-stimulation: a quantitative support for TCR
1249 signalling. *Nat Rev Immunol* **3**, 939-951, doi:10.1038/nri1248 (2003).
1250 39 Lindner, I. *et al.* Induced dendritic cell differentiation of chronic myeloid leukemia blasts
1251 is associated with down-regulation of BCR-ABL. *J Immunol* **171**, 1780-1791 (2003).
1252 40 Townsend, S. E. & Allison, J. P. Tumor rejection after direct costimulation of CD8+ T cells
1253 by B7-transfected melanoma cells. *Science* **259**, 368-370 (1993).
1254 41 Chen, L. *et al.* Costimulation of antitumor immunity by the B7 counterreceptor for the T
1255 lymphocyte molecules CD28 and CTLA-4. *Cell* **71**, 1093-1102 (1992).
1256 42 Wilson, J. L. *et al.* NK cell triggering by the human costimulatory molecules CD80 and
1257 CD86. *J Immunol* **163**, 4207-4212 (1999).
1258 43 Galea-Lauri, J. *et al.* Expression of a variant of CD28 on a subpopulation of human NK
1259 cells: implications for B7-mediated stimulation of NK cells. *J Immunol* **163**, 62-70 (1999).
1260 44 Chambers, B. J., Salcedo, M. & Ljunggren, H. G. Triggering of natural killer cells by the
1261 costimulatory molecule CD80 (B7-1). *Immunity* **5**, 311-317 (1996).
1262 45 Azuma, M., Cayabyab, M., Buck, D., Phillips, J. H. & Lanier, L. L. Involvement of CD28 in
1263 MHC-unrestricted cytotoxicity mediated by a human natural killer leukemia cell line. *J*
1264 *Immunol* **149**, 1115-1123 (1992).
1265 46 Martin-Fontecha, A., Assarsson, E., Carbone, E., Karre, K. & Ljunggren, H. G. Triggering of
1266 murine NK cells by CD40 and CD86 (B7-2). *J Immunol* **162**, 5910-5916 (1999).
1267 47 Peach, R. J. *et al.* Both extracellular immunoglobin-like domains of CD80 contain
1268 residues critical for binding T cell surface receptors CTLA-4 and CD28. *J Biol Chem* **270**,
1269 21181-21187 (1995).
1270 48 Assi, R. *et al.* Final results of a phase 2, open-label study of indisulam, idarubicin, and
1271 cytarabine in patients with relapsed or refractory acute myeloid leukemia and high-risk
1272 myelodysplastic syndrome. *Cancer* **124**, 2758-2765, doi:10.1002/cncr.31398 (2018).
1273 49 Han, T. *et al.* Anticancer sulfonamides target splicing by inducing RBM39 degradation via
1274 recruitment to DCAF15. *Science* **356**, doi:10.1126/science.aal3755 (2017).
1275 50 Uehara, T. *et al.* Selective degradation of splicing factor CAPERalpha by anticancer
1276 sulfonamides. *Nat Chem Biol* **13**, 675-680, doi:10.1038/nchembio.2363 (2017).
1277 51 Ito, T. *et al.* Identification of a primary target of thalidomide teratogenicity. *Science* **327**,
1278 1345-1350, doi:10.1126/science.1177319 (2010).

1279 52 Fischer, E. S. *et al.* Structure of the DDB1-CRBN E3 ubiquitin ligase in complex with
1280 thalidomide. *Nature* **512**, 49-53, doi:10.1038/nature13527 (2014).
1281 53 Kronke, J. *et al.* Lenalidomide causes selective degradation of IKZF1 and IKZF3 in
1282 multiple myeloma cells. *Science* **343**, 301-305, doi:10.1126/science.1244851 (2014).
1283 54 Bolouri, H. *et al.* The molecular landscape of pediatric acute myeloid leukemia reveals
1284 recurrent structural alterations and age-specific mutational interactions. *Nat Med* **24**,
1285 103-112, doi:10.1038/nm.4439 (2018).
1286 55 Cancer Genome Atlas Research, N. *et al.* Genomic and epigenomic landscapes of adult
1287 de novo acute myeloid leukemia. *N Engl J Med* **368**, 2059-2074,
1288 doi:10.1056/NEJMoa1301689 (2013).
1289 56 Roux, K. J., Kim, D. I., Raida, M. & Burke, B. A promiscuous biotin ligase fusion protein
1290 identifies proximal and interacting proteins in mammalian cells. *J Cell Biol* **196**, 801-810,
1291 doi:10.1083/jcb.201112098 (2012).
1292 57 Luo, N. *et al.* Melanoma response to anti-PD-L1 immunotherapy requires JAK1 signaling,
1293 but not JAK2. *Oncoimmunology* **7**, e1438106, doi:10.1080/2162402X.2018.1438106
1294 (2018).
1295 58 Ferlazzo, G. & Munz, C. NK cell compartments and their activation by dendritic cells. *J*
1296 *Immunol* **172**, 1333-1339, doi:10.4049/jimmunol.172.3.1333 (2004).
1297 59 O'Connell, B. C. & Harper, J. W. Ubiquitin proteasome system (UPS): what can chromatin
1298 do for you? *Curr Opin Cell Biol* **19**, 206-214, doi:10.1016/j.ceb.2007.02.014 (2007).
1299 60 Litwin, I., Pilarczyk, E. & Wysocki, R. The Emerging Role of Cohesin in the DNA Damage
1300 Response. *Genes (Basel)* **9**, doi:10.3390/genes9120581 (2018).
1301 61 Chandrashekar, D. S. *et al.* UALCAN: A Portal for Facilitating Tumor Subgroup Gene
1302 Expression and Survival Analyses. *Neoplasia* **19**, 649-658, doi:10.1016/j.neo.2017.05.002
1303 (2017).
1304 62 Doench, J. G. *et al.* Optimized sgRNA design to maximize activity and minimize off-target
1305 effects of CRISPR-Cas9. *Nat Biotechnol* **34**, 184-191, doi:10.1038/nbt.3437 (2016).
1306 63 Sanjana, N. E., Shalem, O. & Zhang, F. Improved vectors and genome-wide libraries for
1307 CRISPR screening. *Nat Methods* **11**, 783-784, doi:10.1038/nmeth.3047 (2014).
1308 64 Grigaite, R., Maneliene, Z. & Janulaitis, A. AarI, a restriction endonuclease from
1309 Arthrobacter aurescens SS2-322, which recognizes the novel non-palindromic sequence
1310 5'-CACCTGC(N)4/8-3'. *Nucleic Acids Res* **30**, e123 (2002).
1311 65 Chen, B. *et al.* Dynamic imaging of genomic loci in living human cells by an optimized
1312 CRISPR/Cas system. *Cell* **155**, 1479-1491, doi:10.1016/j.cell.2013.12.001 (2013).
1313 66 van Overbeek, M. *et al.* DNA Repair Profiling Reveals Nonrandom Outcomes at Cas9-
1314 Mediated Breaks. *Mol Cell* **63**, 633-646, doi:10.1016/j.molcel.2016.06.037 (2016).
1315 67 Stamper, C. C. *et al.* Crystal structure of the B7-1/CTLA-4 complex that inhibits human
1316 immune responses. *Nature* **410**, 608-611, doi:10.1038/35069118 (2001).
1317 68 Patro, R., Duggal, G., Love, M. I., Irizarry, R. A. & Kingsford, C. Salmon provides fast and
1318 bias-aware quantification of transcript expression. *Nat Methods* **14**, 417-419,
1319 doi:10.1038/nmeth.4197 (2017).
1320 69 Pimentel, H., Bray, N. L., Puente, S., Melsted, P. & Pachter, L. Differential analysis of
1321 RNA-seq incorporating quantification uncertainty. *Nat Methods* **14**, 687-690,
1322 doi:10.1038/nmeth.4324 (2017).

1323 70 Barretina, J. *et al.* The Cancer Cell Line Encyclopedia enables predictive modelling of
1324 anticancer drug sensitivity. *Nature* **483**, 603-607, doi:10.1038/nature11003 (2012).
1325 71 Rappsilber, J., Mann, M. & Ishihama, Y. Protocol for micro-purification, enrichment, pre-
1326 fractionation and storage of peptides for proteomics using StageTips. *Nat Protoc* **2**,
1327 1896-1906, doi:10.1038/nprot.2007.261 (2007).
1328 72 Edwards, A. & Haas, W. Multiplexed Quantitative Proteomics for High-Throughput
1329 Comprehensive Proteome Comparisons of Human Cell Lines. *Methods Mol Biol* **1394**, 1-
1330 13, doi:10.1007/978-1-4939-3341-9_1 (2016).
1331 73 Huttlin, E. L. *et al.* A tissue-specific atlas of mouse protein phosphorylation and
1332 expression. *Cell* **143**, 1174-1189, doi:10.1016/j.cell.2010.12.001 (2010).
1333 74 Ting, L., Rad, R., Gygi, S. P. & Haas, W. MS3 eliminates ratio distortion in isobaric
1334 multiplexed quantitative proteomics. *Nat Methods* **8**, 937-940, doi:10.1038/nmeth.1714
1335 (2011).
1336 75 O'Brien, J. J. *et al.* Compositional Proteomics: Effects of Spatial Constraints on Protein
1337 Quantification Utilizing Isobaric Tags. *J Proteome Res* **17**, 590-599,
1338 doi:10.1021/acs.jproteome.7b00699 (2018).
1339 76 Lu, G. *et al.* The myeloma drug lenalidomide promotes the cereblon-dependent
1340 destruction of Ikaros proteins. *Science* **343**, 305-309, doi:10.1126/science.1244917
1341 (2014).
1342

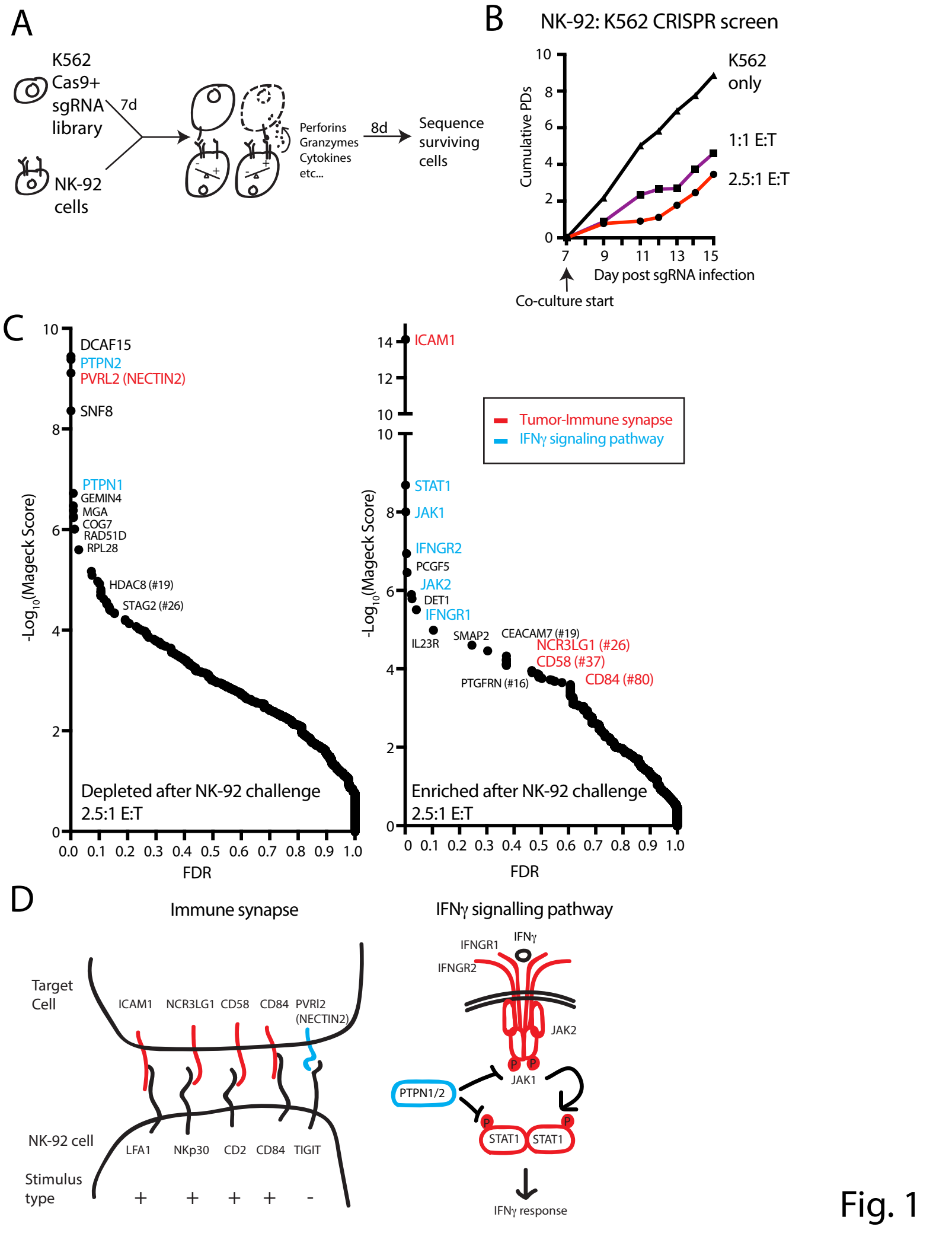
A
K562
Cas9+
sgRNA
library
7d
NK-92
cells
Perforins
Granzymes
Cytokines
etc...
8d
Sequence
surviving
cells
B
NK-92: K562 CRISPR screen
Cumulative PDs
K562
only
1:1 E:T
2.5:1 E:T
Day post sgRNA infection
Co-culture start
C
DCAF15
PTPN2
PVRL2 (NECTIN2)
SNF8
PTPN1
GEMIN4
MGA
COG7
RAD51D
RPL28
HDAC8 (#19)
STAG2 (#26)
-Log10(Mageck Score)
Depleted after NK-92 challenge
2.5:1 E:T
FDR
ICAM1
Tumor-Immune synapse
IFNγ signaling pathway
STAT1
JAK1
IFNGR2
PCGF5
JAK2
DET1
IFNGR1
IL23R
SMAP2
CEACAM7 (#19)
NCR3LG1 (#26)
CD58 (#37)
CD84 (#80)
PTGFRN (#16)
Enriched after NK-92 challenge
2.5:1 E:T
D
Immune synapse
Target
Cell
ICAM1
NCR3LG1
CD58
CD84
PVRl2
(NECTIN2)
NK-92 cell
LFA1
NKp30
CD2
CD84
TIGIT
Stimulus
type
IFNγ signalling pathway
IFNγ
IFNGR1
IFNGR2
JAK2
JAK1
PTPN1/2
STAT1
STAT1
IFNγ response

Fig. 1

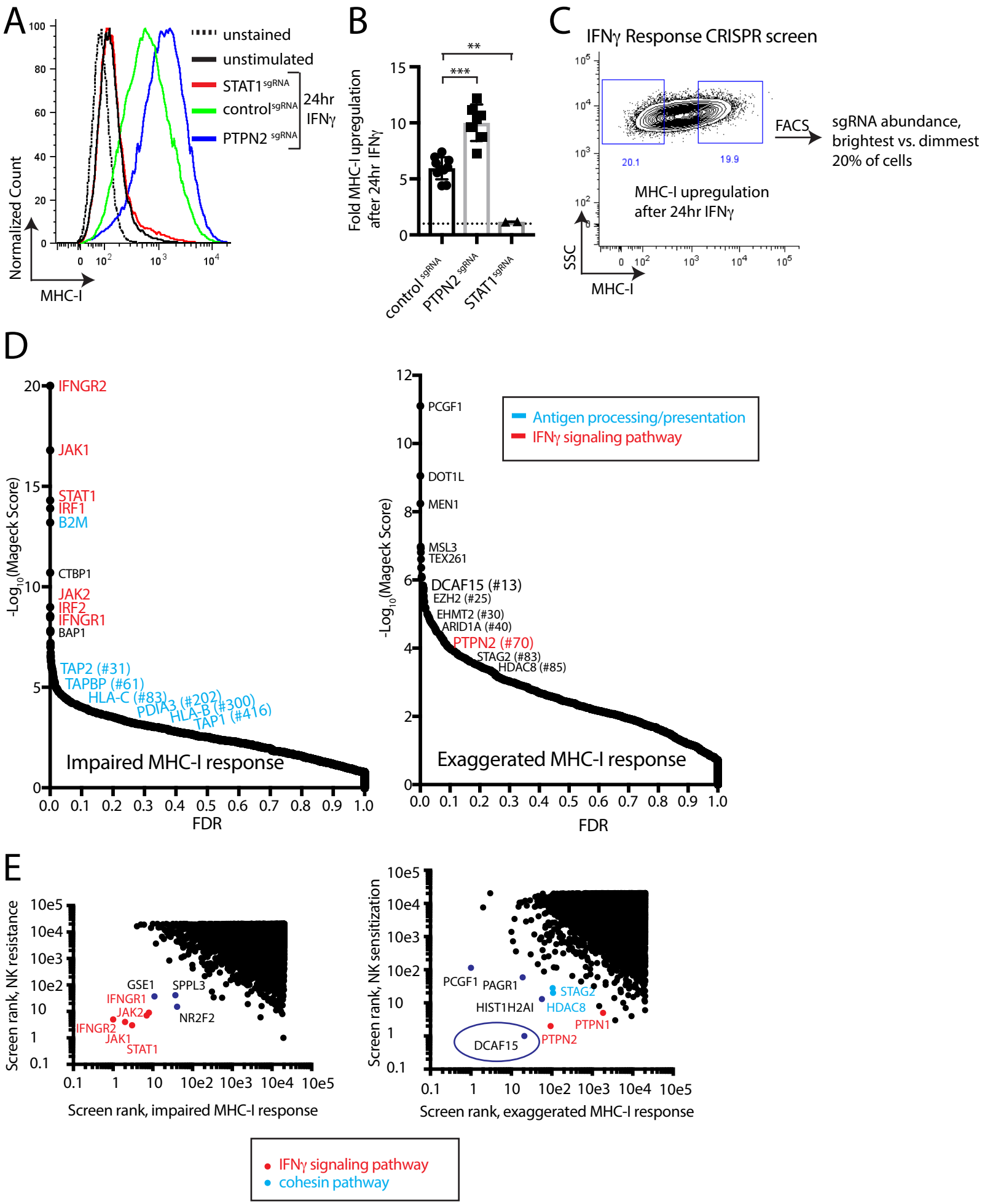
A
unstained
unstimulated
STAT1 sgRNA
control sgRNA
PTPN2 sgRNA
24hr IFNγ
Normalized Count
MHC-I
B
Fold MHC-I upregulation after 24hr IFNγ
control sgRNA
PTPN2 sgRNA
STAT1 sgRNA
C
IFNγ Response CRISPR screen
FACS
sgRNA abundance, brightest vs. dimmest 20% of cells
20.1
19.9
MHC-I upregulation after 24hr IFNγ
SSC
MHC-I
D
IFNGR2
JAK1
STAT1
IRF1
B2M
CTBP1
JAK2
IRF2
IFNGR1
BAP1
TAP2 (#31)
TAPBP (#61)
HLA-C (#83)
PDIA3 (#202)
HLA-B (#300)
TAP1 (#416)
Impaired MHC-I response
-Log10(Mageck Score)
FDR
Antigen processing/presentation
IFNγ signaling pathway
PCGF1
DOT1L
MEN1
MSL3
TEX261
DCAF15 (#13)
EZH2 (#25)
EHMT2 (#30)
ARID1A (#40)
PTPN2 (#70)
STAG2 (#83)
HDAC8 (#85)
Exaggerated MHC-I response
E
Screen rank, NK resistance
GSE1
SPPL3
IFNGR1
JAK2
NR2F2
IFNGR2
JAK1
STAT1
Screen rank, impaired MHC-I response
Screen rank, NK sensitization
PCGF1
PAGR1
STAG2
HIST1H2AI
HDAC8
PTPN1
PTPN2
DCAF15
Screen rank, exaggerated MHC-I response
IFNγ signaling pathway
cohesin pathway

Fig. 2

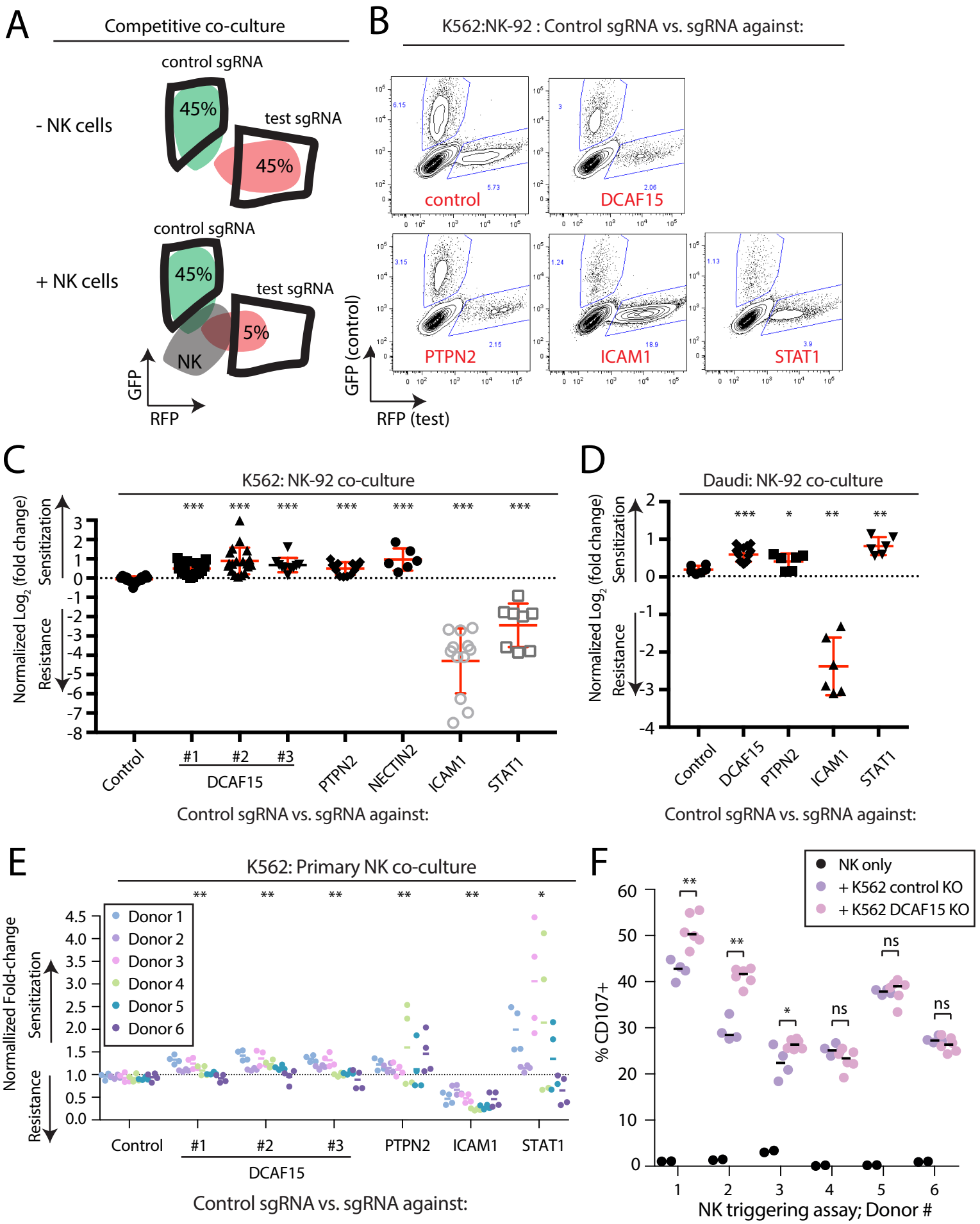
A
Competitive co-culture
control sgRNA
- NK cells
45%
test sgRNA
45%
control sgRNA
+ NK cells
45%
test sgRNA
5%
NK
GFP
RFP
B
K562:NK-92 : Control sgRNA vs. sgRNA against:
control
DCAF15
PTPN2
ICAM1
STAT1
GFP (control)
RFP (test)
C
K562: NK-92 co-culture
Normalized Log2 (fold change)
Sensitization
Resistance
Control
#1
#2
#3
DCAF15
PTPN2
NECTIN2
ICAM1
STAT1
Control sgRNA vs. sgRNA against:
D
Daudi: NK-92 co-culture
Normalized Log2 (fold change)
Sensitization
Resistance
Control
DCAF15
PTPN2
ICAM1
STAT1
Control sgRNA vs. sgRNA against:
E
K562: Primary NK co-culture
Normallized Fold-change
Sensitization
Resistance
Donor 1
Donor 2
Donor 3
Donor 4
Donor 5
Donor 6
Control
#1
#2
#3
DCAF15
PTPN2
ICAM1
STAT1
Control sgRNA vs. sgRNA against:
F
NK only
+ K562 control KO
+ K562 DCAF15 KO
% CD107+
NK triggering assay; Donor #

Fig. 3

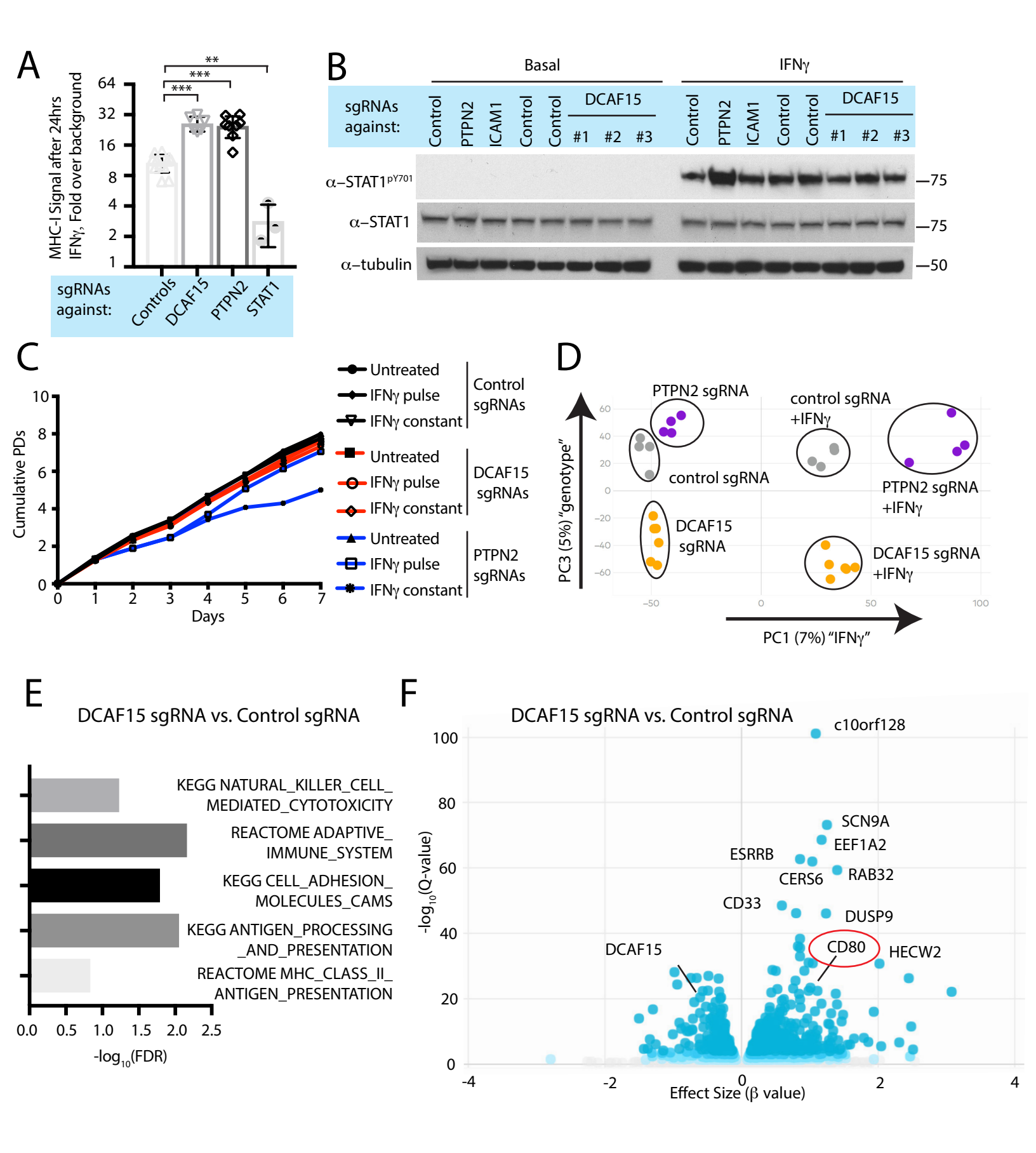
A
MHC-I Signal after 24hrs IFNγ, Fold over background
64
32
16
8
4
2
1
**
***
***
sgRNAs against:
Controls
DCAF15
PTPN2
STAT1
B
Basal
IFNγ
sgRNAs against:
Control
PTPN2
ICAM1
Control
Control
DCAF15
#1
#2
#3
α–STAT1pY701
α–STAT1
α–tubulin
—75
—75
—50
C
Cumulative PDs
Days
Untreated
IFNγ pulse
IFNγ constant
Control sgRNAs
DCAF15 sgRNAs
PTPN2 sgRNAs
D
PTPN2 sgRNA
control sgRNA
control sgRNA +IFNγ
PTPN2 sgRNA +IFNγ
DCAF15 sgRNA
DCAF15 sgRNA +IFNγ
PC3 (5%) "genotype"
PC1 (7%) "IFNγ"
E
DCAF15 sgRNA vs. Control sgRNA
KEGG NATURAL_KILLER_CELL_MEDIATED_CYTOTOXICITY
REACTOME ADAPTIVE_IMMUNE_SYSTEM
KEGG CELL_ADHESION_MOLECULES_CAMS
KEGG ANTIGEN_PROCESSING_AND_PRESENTATION
REACTOME MHC_CLASS_II_ANTIGEN_PRESENTATION
-log10(FDR)
F
DCAF15 sgRNA vs. Control sgRNA
c10orf128
SCN9A
EEF1A2
ESRRB
CERS6
RAB32
CD33
DUSP9
CD80
HECW2
DCAF15
-log10(Q-value)
Effect Size (β value)

Fig. 4

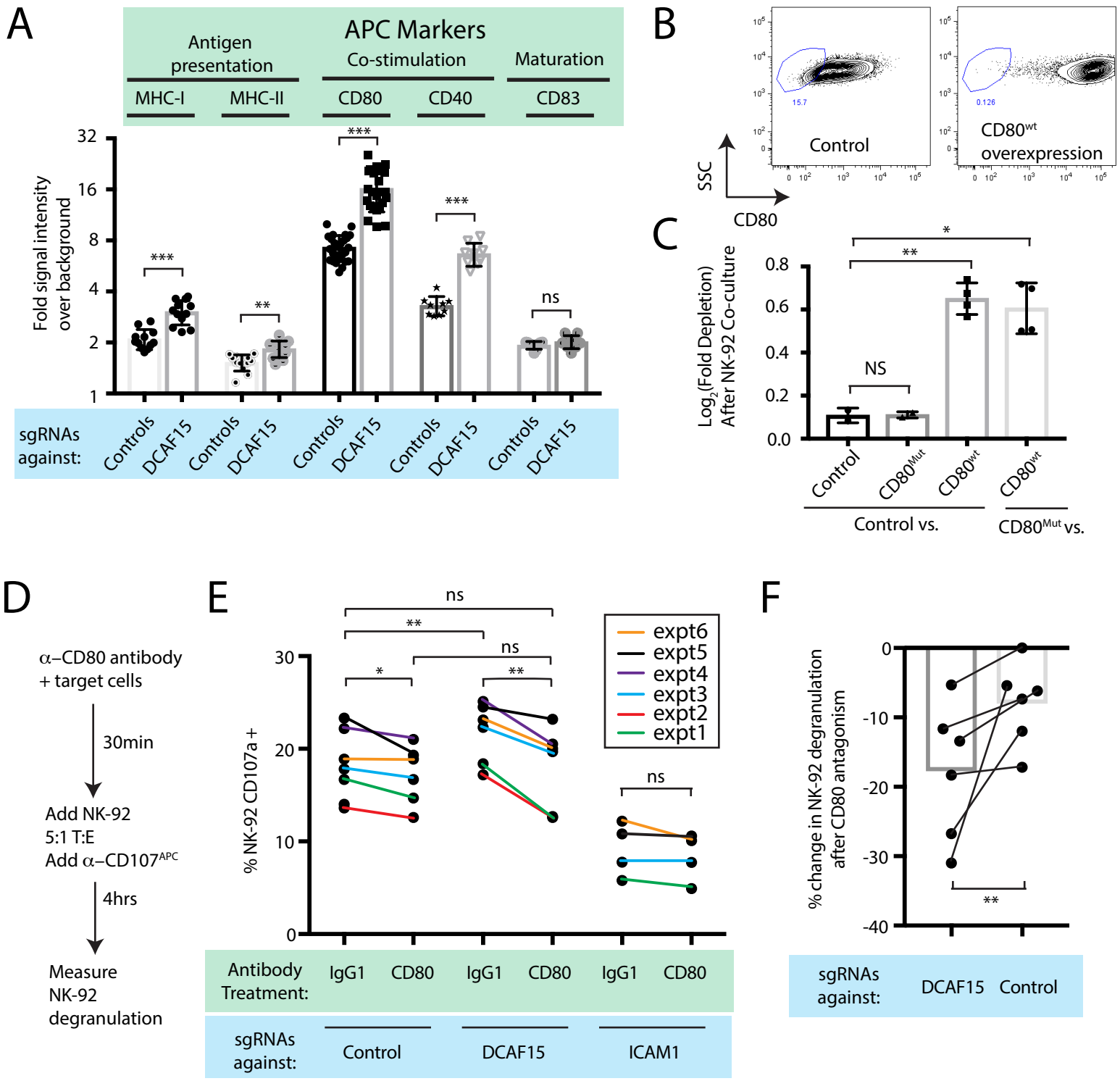
A
APC Markers
Antigen presentation
Co-stimulation
Maturation
MHC-I
MHC-II
CD80
CD40
CD83
Fold signal intensity over background
32
16
8
4
2
1
***
**
***
***
ns
sgRNAs against:
Controls
DCAF15
B
SSC
CD80
Control
CD80wt overexpression
C
Log2(Fold Depletion) After NK-92 Co-culture
0.8
0.6
0.4
0.2
0.0
*
**
NS
Control
CD80Mut
CD80wt
Control vs.
CD80Mut vs.
D
α–CD80 antibody + target cells
30min
Add NK-92 5:1 T:E
Add α–CD107APC
4hrs
Measure NK-92 degranulation
E
% NK-92 CD107a +
30
20
10
0
ns
**
*
expt6
expt5
expt4
expt3
expt2
expt1
Antibody Treatment:
IgG1
CD80
sgRNAs against:
Control
DCAF15
ICAM1
F
% change in NK-92 degranulation after CD80 antagonism
0
-10
-20
-30
-40
**
sgRNAs against:
DCAF15
Control

Fig. 5

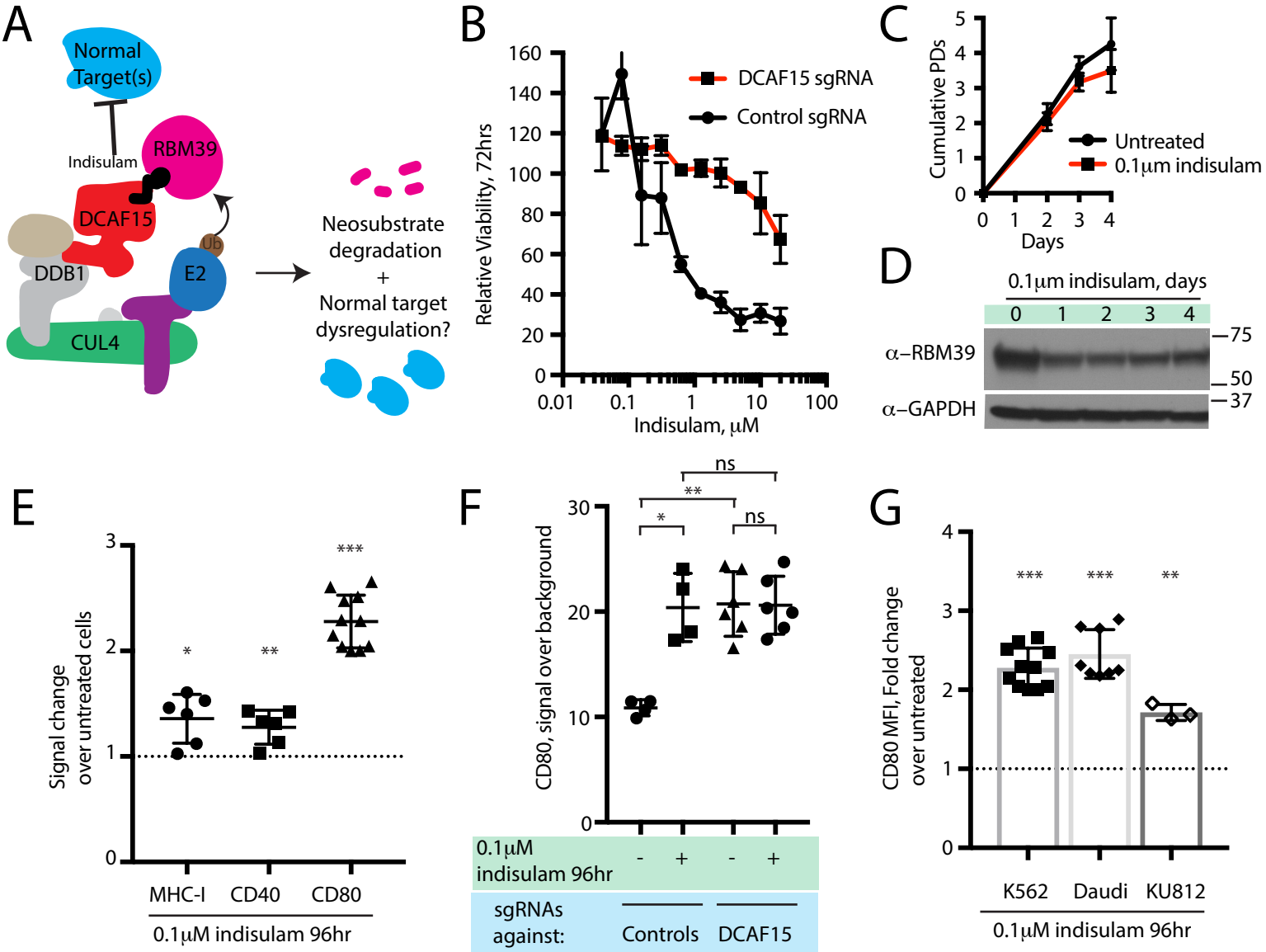
A
Normal Target(s)
Indisulam
RBM39
DCAF15
DDB1
E2
Ub
CUL4
Neosubstrate degradation + Normal target dysregulation?
B
DCAF15 sgRNA
Control sgRNA
Relative Viability, 72hrs
Indisulam, μM
C
Cumulative PDs
Untreated
0.1μm indisulam
Days
D
0.1μm indisulam, days
0 1 2 3 4
α–RBM39
α–GAPDH
75
50
37
E
Signal change over untreated cells
MHC-I
CD40
CD80
0.1μM indisulam 96hr
F
CD80, signal over background
ns
**
*
ns
0.1μM indisulam 96hr
sgRNAs against:
Controls
DCAF15
G
CD80 MFI, Fold change over untreated
K562
Daudi
KU812
0.1μM indisulam 96hr

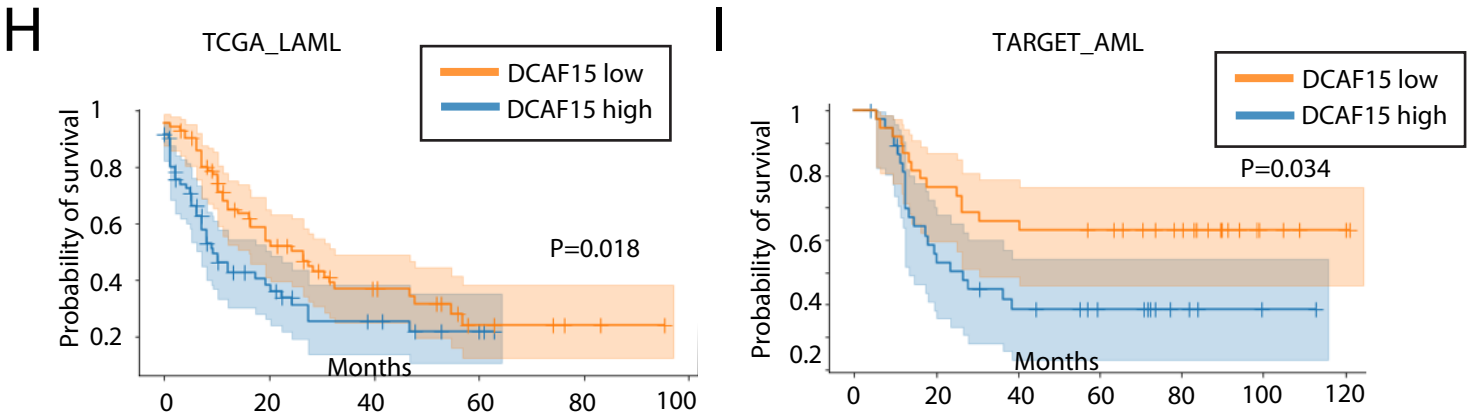
H
TCGA_LAML
DCAF15 low
DCAF15 high
Probability of survival
P=0.018
Months
I
TARGET_AML
DCAF15 low
DCAF15 high
Probability of survival
P=0.034
Months

Fig. 6

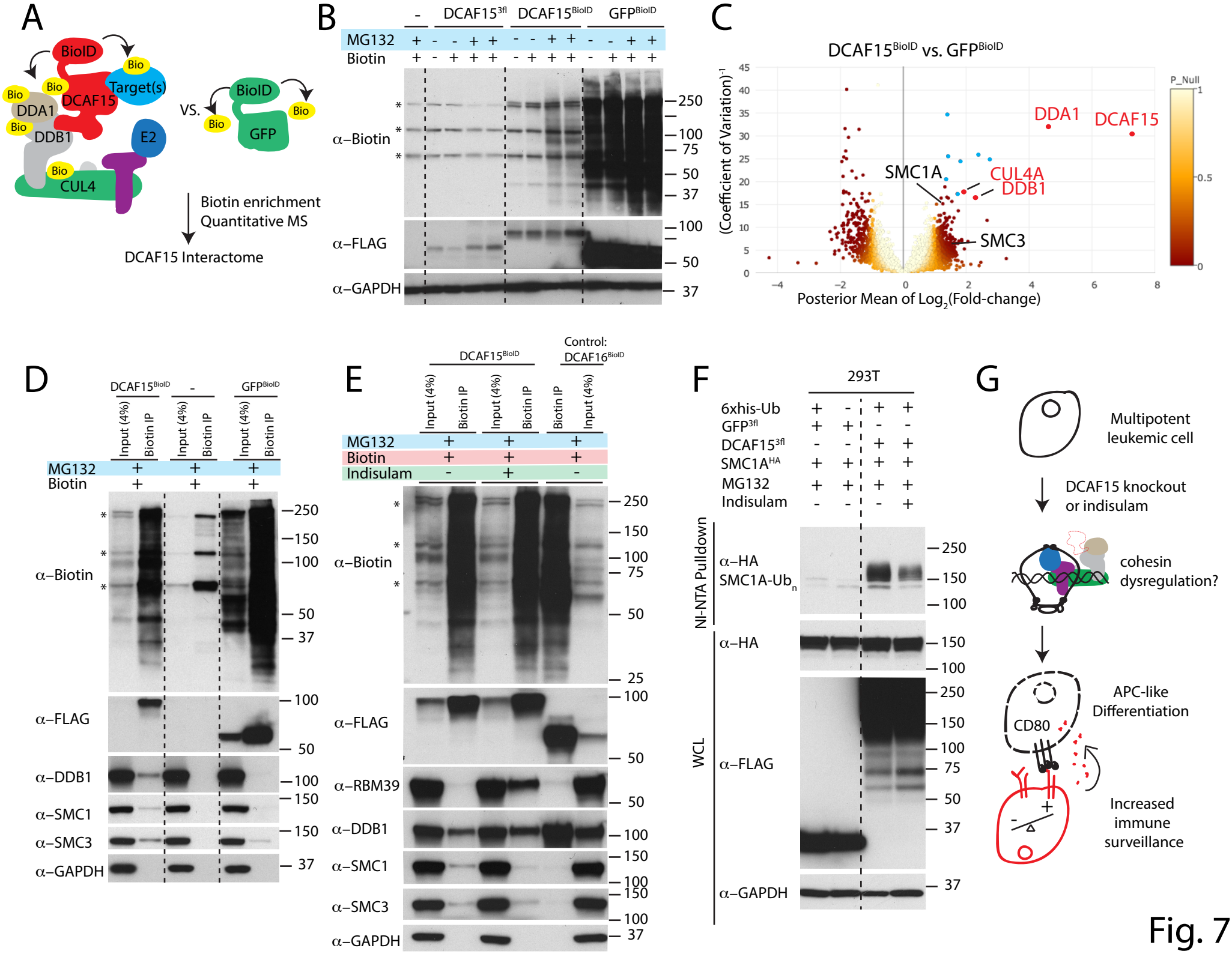
A
BioID
Bio
Target(s)
DCAF15
DDA1
DDB1
E2
CUL4
VS.
GFP
Biotin enrichment
Quantitative MS
DCAF15 Interactome
B
DCAF15^3fl
DCAF15^BioID
GFP^BioID
MG132
Biotin
α–Biotin
α–FLAG
α–GAPDH
C
DCAF15^BioID vs. GFP^BioID
(Coefficient of Variation)^-1
Posterior Mean of Log2(Fold-change)
P_Null
DDA1
DCAF15
SMC1A
CUL4A
DDB1
SMC3
D
DCAF15^BioID
GFP^BioID
Input (4%)
Biotin IP
α–Biotin
α–FLAG
α–DDB1
α–SMC1
α–SMC3
α–GAPDH
E
Control: DCAF16^BioID
Indisulam
α–RBM39
F
293T
6xhis-Ub
GFP^3fl
DCAF15^3fl
SMC1A^HA
Indisulam
Ni-NTA Pulldown
WCL
α–HA
SMC1A-Ub_n
G
Multipotent leukemic cell
DCAF15 knockout or indisulam
cohesin dysregulation?
APC-like Differentiation
CD80
Increased immune surveillance

Fig. 7

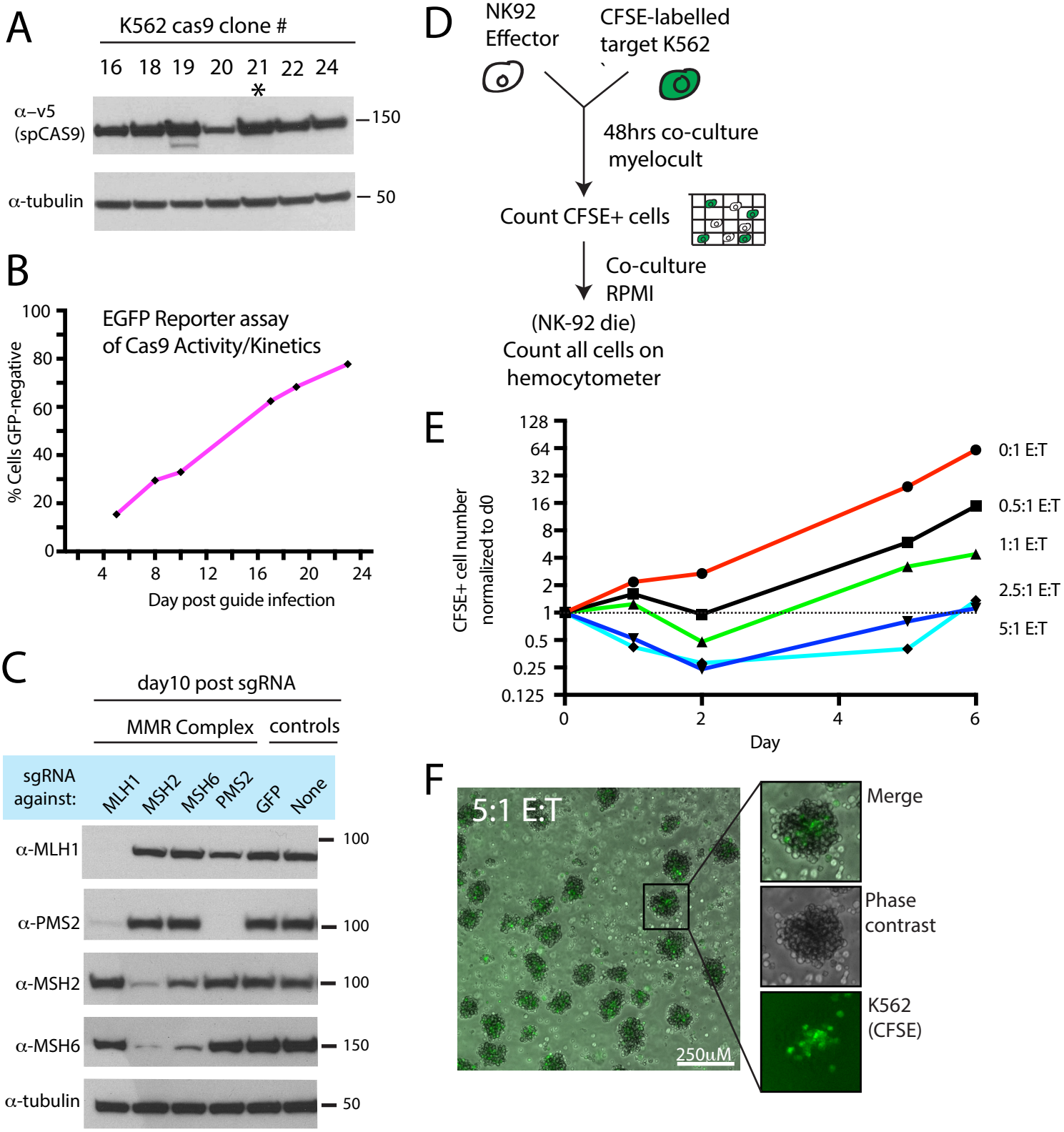
A
K562 cas9 clone #
16 18 19 20 21 22 24
*
α–v5 (spCAS9)
150
α-tubulin
50
B
EGFP Reporter assay of Cas9 Activity/Kinetics
% Cells GFP-negative
Day post guide infection
C
day10 post sgRNA
MMR Complex
controls
sgRNA against:
MLH1 MSH2 MSH6 PMS2 GFP None
α-MLH1
α-PMS2
α-MSH2
α-MSH6
α-tubulin
D
NK92 Effector
CFSE-labelled target K562
48hrs co-culture myelocult
Count CFSE+ cells
Co-culture RPMI
(NK-92 die)
Count all cells on hemocytometer
E
CFSE+ cell number normalized to d0
Day
0:1 E:T
0.5:1 E:T
1:1 E:T
2.5:1 E:T
5:1 E:T
F
5:1 E:T
250µM
Merge
Phase contrast
K562 (CFSE)

Fig1- S1

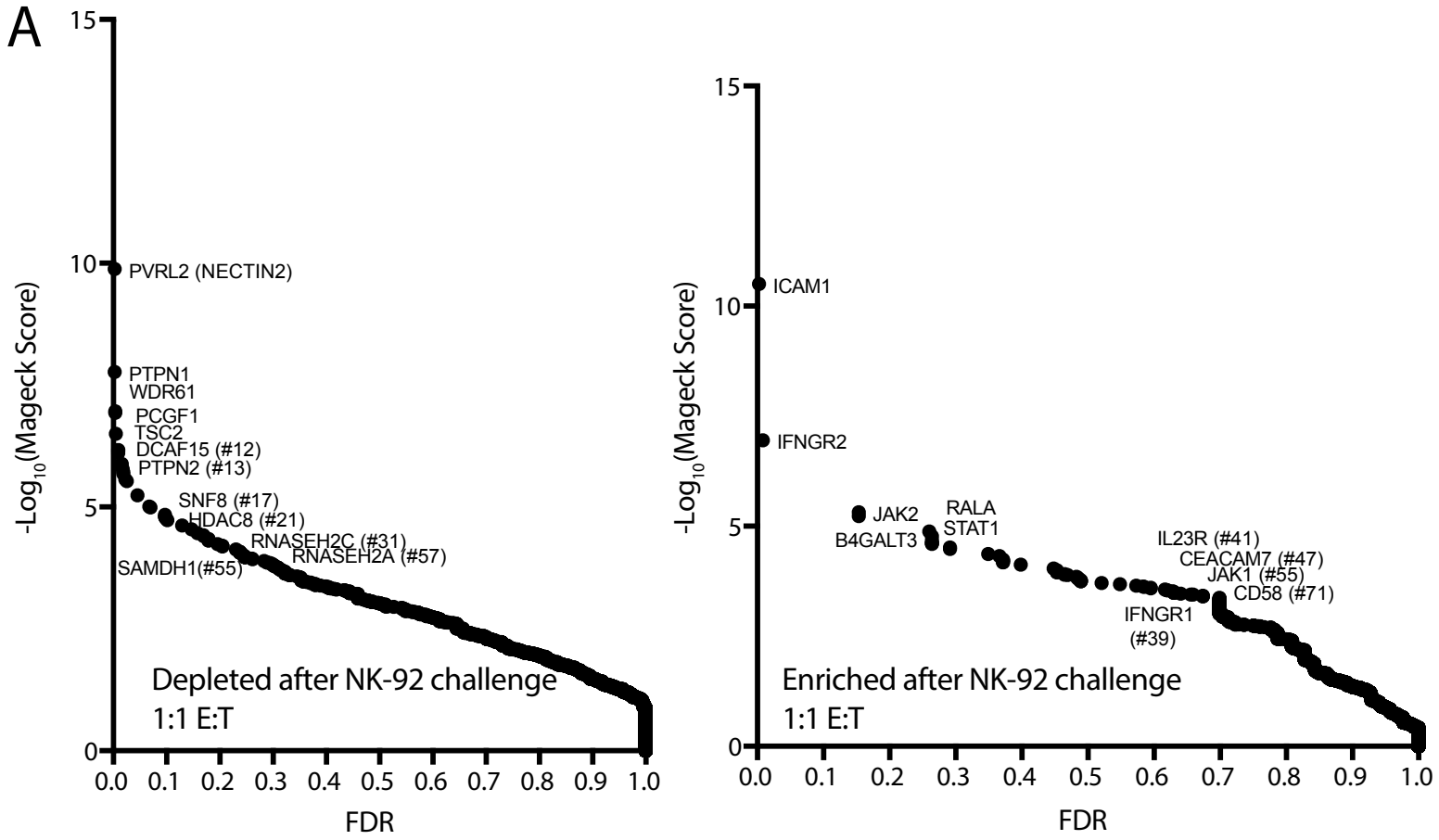
A
15
10
5
0
-Log10(Mageck Score)
PVRL2 (NECTIN2)
PTPN1
WDR61
PCGF1
TSC2
DCAF15 (#12)
PTPN2 (#13)
SNF8 (#17)
HDAC8 (#21)
RNASEH2C (#31)
RNASEH2A (#57)
SAMDH1(#55)
Depleted after NK-92 challenge
1:1 E:T
0.0 0.1 0.2 0.3 0.4 0.5 0.6 0.7 0.8 0.9 1.0
FDR
ICAM1
IFNGR2
JAK2
RALA
STAT1
B4GALT3
IL23R (#41)
CEACAM7 (#47)
JAK1 (#55)
CD58 (#71)
IFNGR1
(#39)
Enriched after NK-92 challenge
1:1 E:T

Fig1-S2

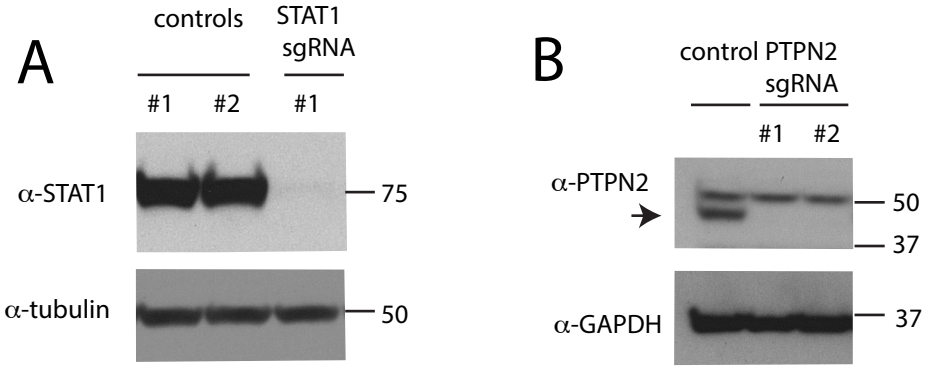
A
controls
STAT1 sgRNA
#1
#2
#1
α-STAT1
75
α-tubulin
50
B
control
PTPN2 sgRNA
#1
#2
α-PTPN2
50
37
α-GAPDH
37

Fig2-S1

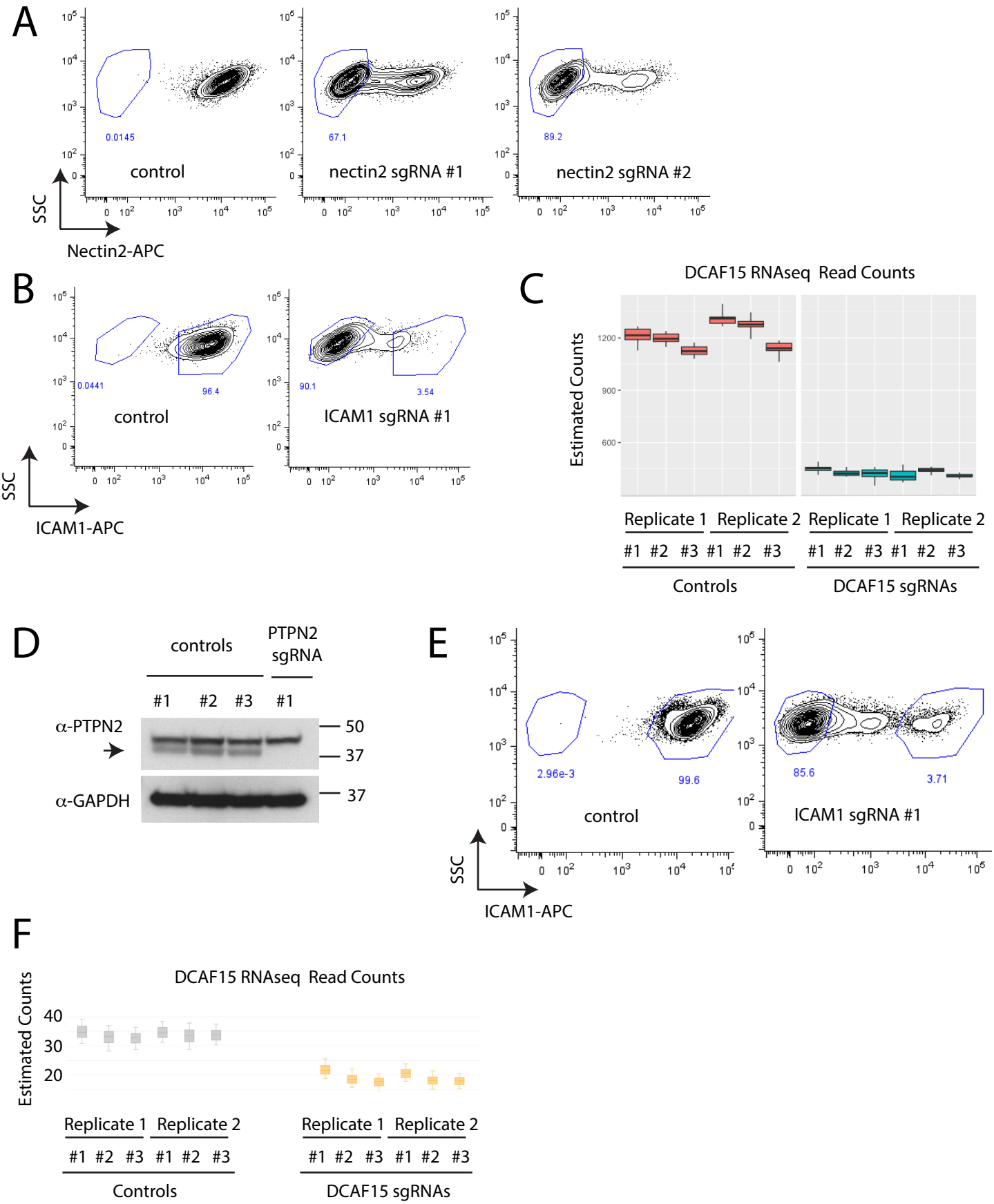
A
0.0145
control
67.1
nectin2 sgRNA #1
89.2
nectin2 sgRNA #2
SSC
Nectin2-APC
B
0.0441
96.4
control
90.1
3.54
ICAM1 sgRNA #1
SSC
ICAM1-APC
C
DCAF15 RNAseq Read Counts
Estimated Counts
Replicate 1 Replicate 2 Replicate 1 Replicate 2
#1 #2 #3 #1 #2 #3 #1 #2 #3 #1 #2 #3
Controls
DCAF15 sgRNAs
D
controls
PTPN2 sgRNA
#1 #2 #3 #1
α-PTPN2
50
37
α-GAPDH
37
E
2.96e-3
99.6
control
85.6
3.71
ICAM1 sgRNA #1
SSC
ICAM1-APC
F
DCAF15 RNAseq Read Counts
Estimated Counts
Replicate 1 Replicate 2 Replicate 1 Replicate 2
#1 #2 #3 #1 #2 #3 #1 #2 #3 #1 #2 #3
Controls
DCAF15 sgRNAs

Fig.3-S1

A

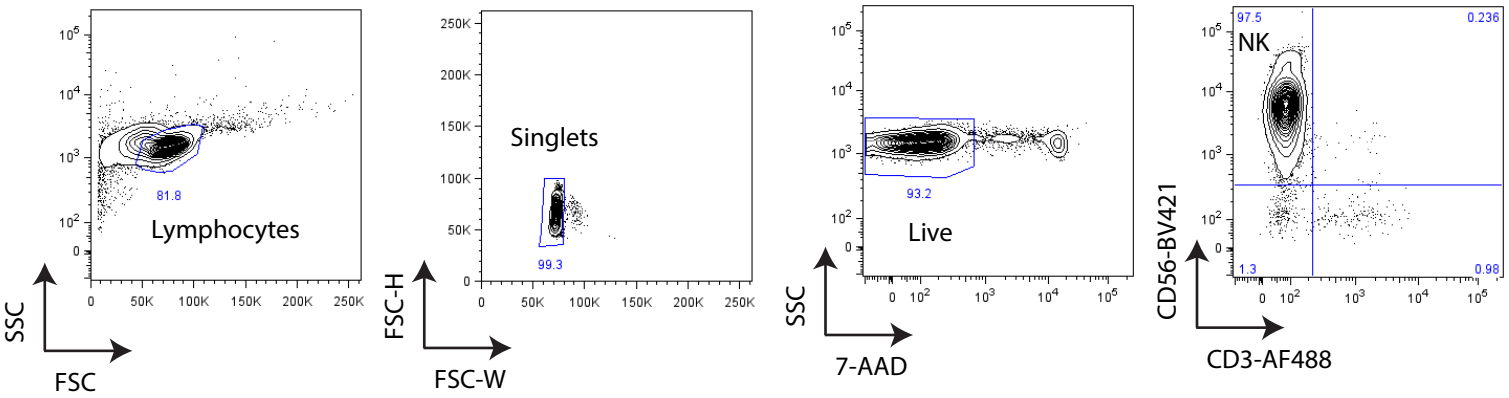
Lymphocytes
81.8
SSC
FSC
Singlets
99.3
FSC-H
FSC-W
Live
93.2
SSC
7-AAD
NK
97.5
0.236
1.3
0.98
CD56-BV421
CD3-AF488

B

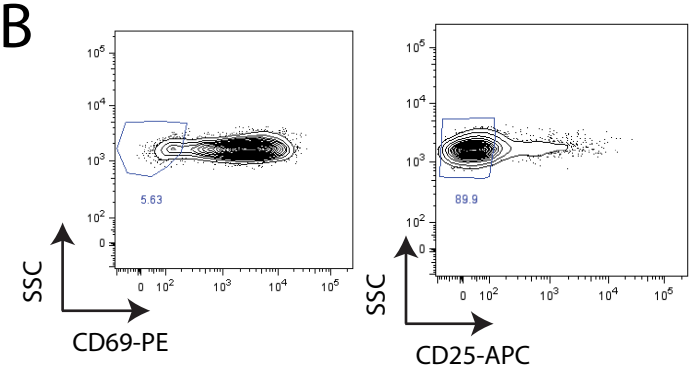
5.63
SSC
CD69-PE
89.9
SSC
CD25-APC

Fig.3-S2

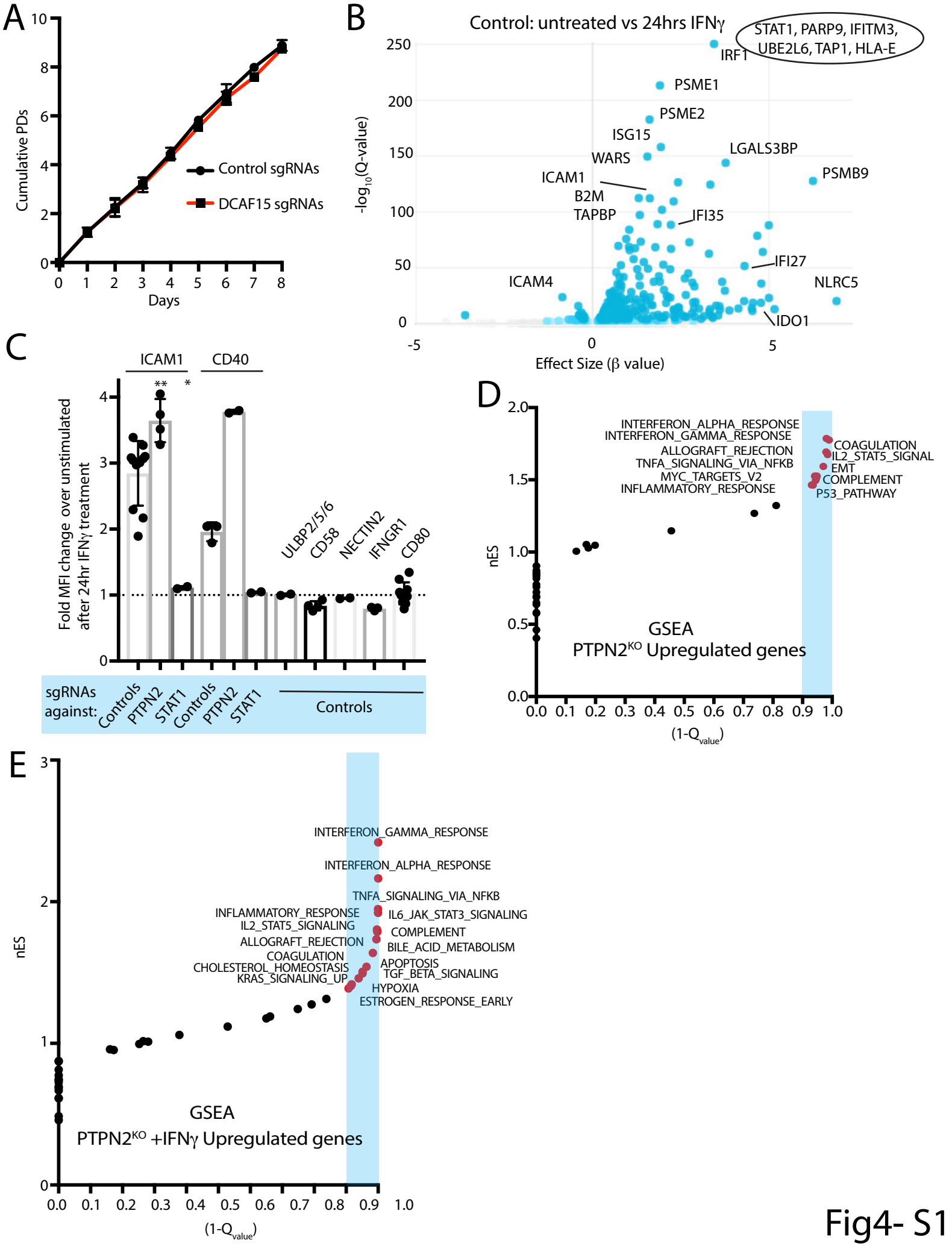
A
Cumulative PDs
Days
Control sgRNAs
DCAF15 sgRNAs
B
Control: untreated vs 24hrs IFNγ
STAT1, PARP9, IFITM3, UBE2L6, TAP1, HLA-E
IRF1
PSME1
PSME2
ISG15
WARS
LGALS3BP
PSMB9
ICAM1
B2M
TAPBP
IFI35
IFI27
ICAM4
NLRC5
IDO1
-log10(Q-value)
Effect Size (β value)
C
ICAM1
CD40
ULBP2/5/6
CD58
NECTIN2
IFNGR1
CD80
Fold MFI change over unstimulated after 24hr IFNγ treatment
sgRNAs against:
Controls
PTPN2
STAT1
Controls
PTPN2
STAT1
Controls
D
INTERFERON_ALPHA_RESPONSE
INTERFERON_GAMMA_RESPONSE
ALLOGRAFT_REJECTION
TNFA_SIGNALING_VIA_NFKB
MYC_TARGETS_V2
INFLAMMATORY_RESPONSE
COAGULATION
IL2_STAT5_SIGNAL
EMT
COMPLEMENT
P53_PATHWAY
nES
GSEA
PTPN2KO Upregulated genes
(1-Qvalue)
E
INTERFERON_GAMMA_RESPONSE
INTERFERON_ALPHA_RESPONSE
TNFA_SIGNALING_VIA_NFKB
INFLAMMATORY_RESPONSE
IL6_JAK_STAT3_SIGNALING
IL2_STAT5_SIGNALING
COMPLEMENT
ALLOGRAFT_REJECTION
BILE_ACID_METABOLISM
COAGULATION
APOPTOSIS
CHOLESTEROL_HOMEOSTASIS
TGF_BETA_SIGNALING
KRAS_SIGNALING_UP
HYPOXIA
ESTROGEN_RESPONSE_EARLY
nES
GSEA
PTPN2KO +IFNγ Upregulated genes
(1-Qvalue)

Fig4- S1

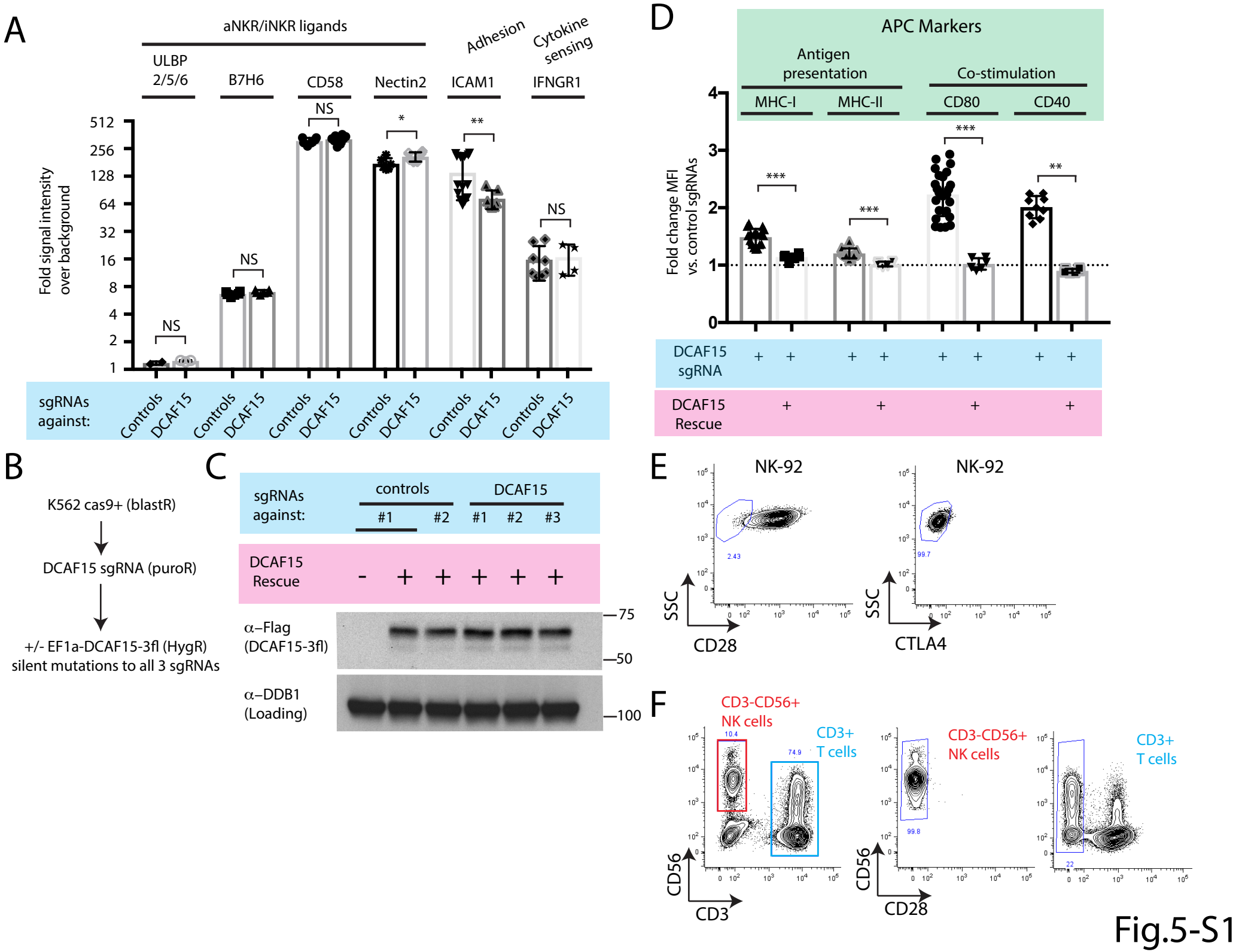
A
aNKR/iNKR ligands
Adhesion
Cytokine sensing
ULBP 2/5/6
B7H6
CD58
Nectin2
ICAM1
IFNGR1
Fold signal intensity over background
512
256
128
64
32
16
8
4
2
1
NS
NS
NS
*
**
NS
sgRNAs against:
Controls
DCAF15
B
K562 cas9+ (blastR)
DCAF15 sgRNA (puroR)
+/- EF1a-DCAF15-3fl (HygR)
silent mutations to all 3 sgRNAs
C
sgRNAs against:
controls
DCAF15
#1
#2
#3
DCAF15 Rescue
α–Flag (DCAF15-3fl)
α–DDB1 (Loading)
75
50
100
D
APC Markers
Antigen presentation
Co-stimulation
MHC-I
MHC-II
CD80
CD40
Fold change MFI vs. control sgRNAs
***
***
***
**
DCAF15 sgRNA
DCAF15 Rescue
E
NK-92
NK-92
SSC
CD28
CTLA4
2.43
99.7
F
CD3-CD56+ NK cells
CD3+ T cells
CD56
CD3
CD28
10.4
74.9
99.8
22

Fig.5-S1

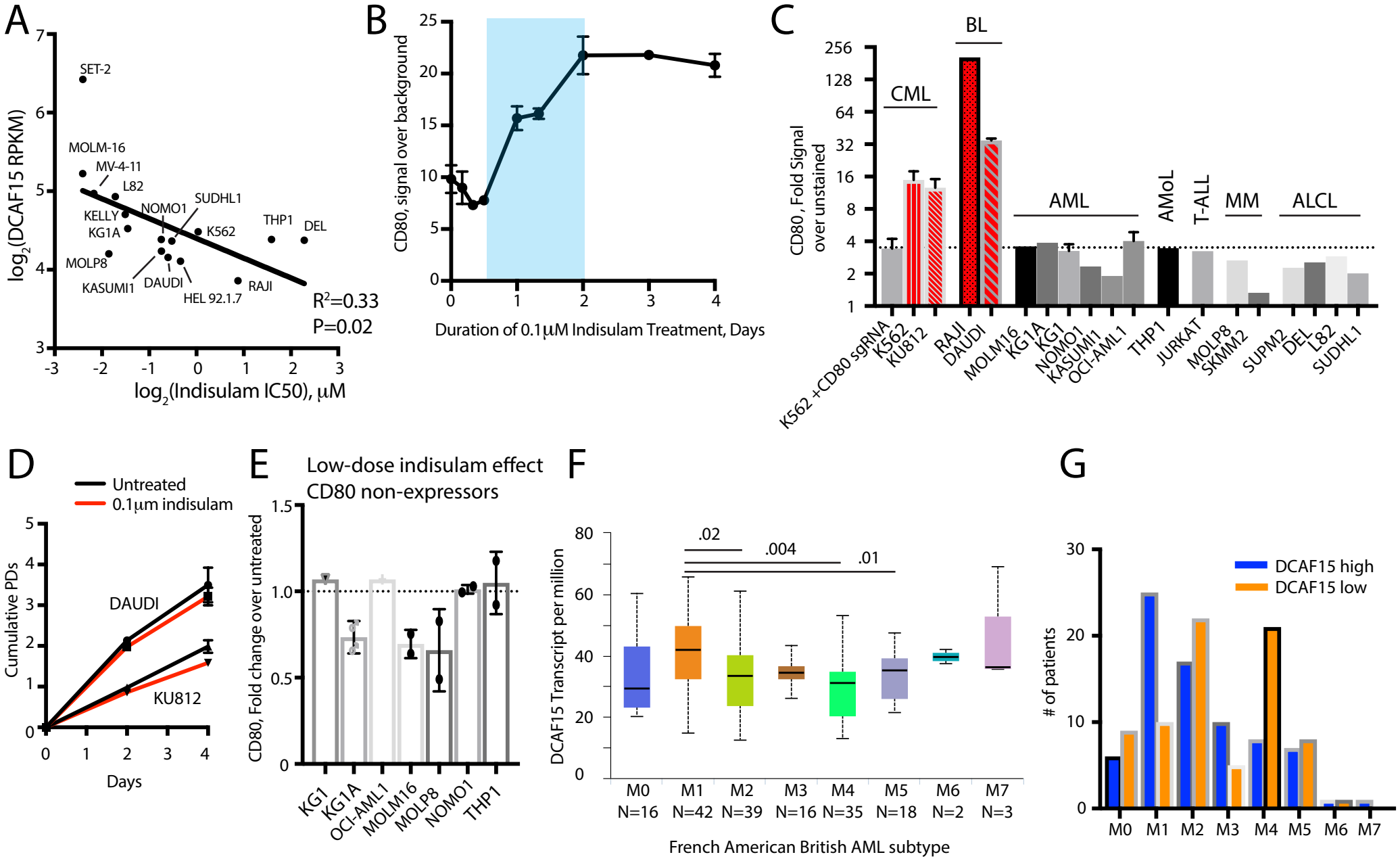
A
log2(DCAF15 RPKM)
log2(Indisulam IC50), μM
SET-2
MOLM-16
MV-4-11
L82
KELLY
KG1A
NOMO1
SUDHL1
K562
THP1
DEL
MOLP8
KASUMI1
DAUDI
HEL 92.1.7
RAJI
R2=0.33
P=0.02
B
CD80, signal over background
Duration of 0.1μM Indisulam Treatment, Days
C
CD80 , Fold Signal over unstained
CML
BL
AML
AMoL
T-ALL
MM
ALCL
K562 +CD80 sgRNA
K562
KU812
RAJI
DAUDI
MOLM16
KG1A
KG1
NOMO1
KASUMI1
OCI-AML1
THP1
JURKAT
MOLP8
SKMM2
SUPM2
DEL
L82
SUDHL1
D
Untreated
0.1μm indisulam
Cumulative PDs
DAUDI
KU812
Days
E
Low-dose indisulam effect
CD80 non-expressors
CD80, Fold change over untreated
KG1
KG1A
OCI-AML1
MOLM16
MOLP8
NOMO1
THP1
F
DCAF15 Transcript per million
.02
.004
.01
M0 N=16
M1 N=42
M2 N=39
M3 N=16
M4 N=35
M5 N=18
M6 N=2
M7 N=3
French American British AML subtype
G
DCAF15 high
DCAF15 low
# of patients
M0
M1
M2
M3
M4
M5
M6
M7

Fig.6-S1

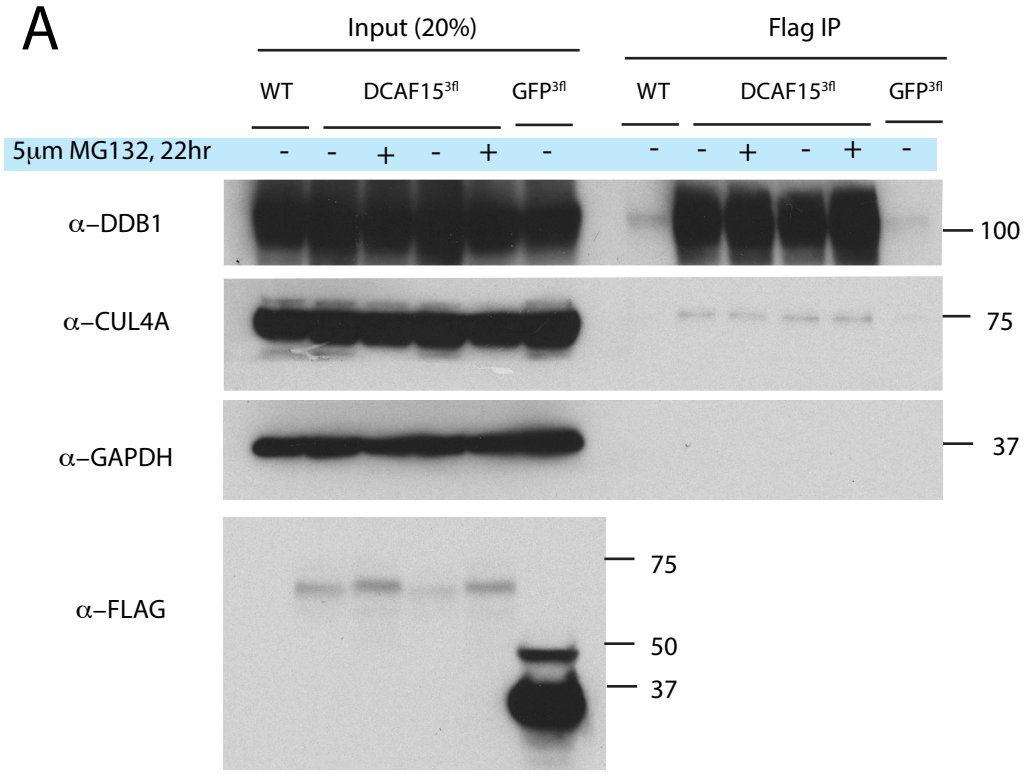
A
Input (20%)
Flag IP
WT
DCAF15^{3fl}
GFP^{3fl}
WT
DCAF15^{3fl}
GFP^{3fl}
5μm MG132, 22hr
- - + - + -
- - + - + -
α–DDB1
100
α–CUL4A
75
α–GAPDH
37
α–FLAG
75
50
37

Fig.7-S1